MAPPING CORTICOSTRIATAL SYNAPSES ONTO SPINY PROJECTION NEURONS

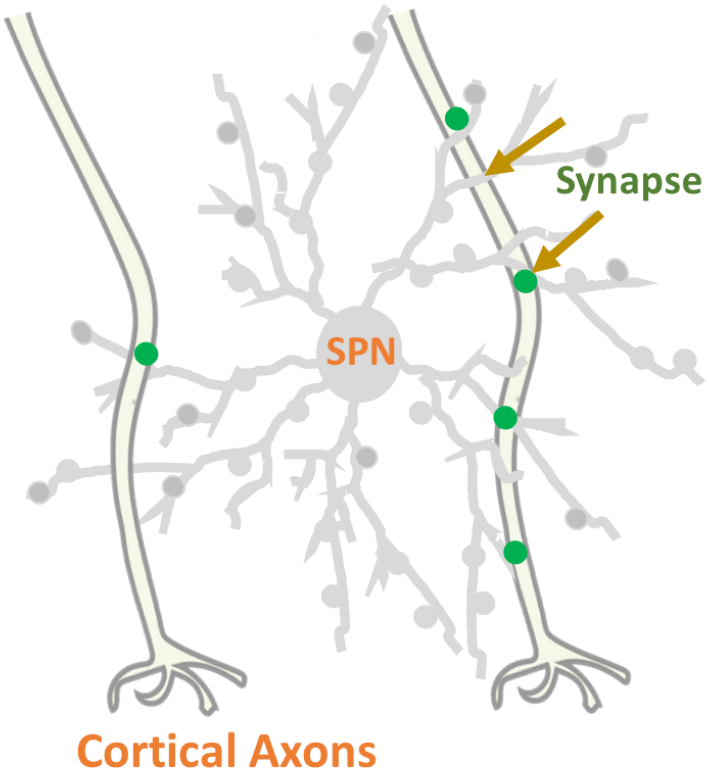

ANA FILIPA POMBINHO ISIDRO

A dissertation submitted in partial fulfillment of the requirements for the Degree of Master's in Biomedical Research

Dissertação para obtenção do grau de Mestre em Investigação Biomédica

at Faculdade de Ciências Médicas | NOVA Medical School of NOVA University Lisbon

September 2019

MAPPING CORTICOSTRIATAL SYNAPSES ONTO SPINY PROJECTION NEURONS

Ana Filipa Pombinho Isidro

Supervisors: Daniela Pereira, PhD; Nicolas Morgenstern, PhD and Rui Costa, DMV and PhD of Champalimaud Foundation

A dissertation submitted in partial fulfillment of the requirements for the Degree of Master's in Biomedical Research

Dissertação para obtenção do grau de Mestre em Investigação Biomédica

September 2019

Acknowledgments

First, I would like to thank my supervisors for giving me this amazing opportunity. Rui Costa, for allowing to take part of this extraordinary lab and meet wonderful scientists and future peers. Daniela Pereira and Nicolas Morgenstern, for the advice, the help and scientific debates that I cherished with you. You both taught me more than I ever imaged a master student could learn. You guided me during this project, but also allowed me to actively contribute with alternatives and possible methodologies to approach the problems we faced. I am also thankful for all your life advices and possible future prospects you recommended to me.

I kindly thank Loredana Stoica and Cristina Álcacer for their emotional support throughout this journey. Lori, you have shown me new ways to deal with my anxieties and insecurities, I am very thankful for having your support. I also thank all the other members of the Costa Lab, for all the conversations, help and advise you gave throughout the year. I am very grateful to have met you all, you are extraordinary people to work with, you were always available to help finding tools, reagents, software and help with data analysis in case I needed it. I also want to thank Margarida Pinto, the new naive master student, to whom I shared concerns and laughs during our 'short coffee breaks'.

Inês Dias, Ana Rasteiro, Raquel Soares, Raquel Silva e Gonçalo Malpica, vocês são excelentes pessoas. Obrigado por todas as risadas, histórias e apoio partilhado durante o ano. Foi um ano longo, mas juntos iremos celebrar este ano como mais uma etapa conquistada.

Leonor Morgado e Sara Abalde, obrigado por todas as pausas do café e idas ao ginásio, que, entretanto, se perderam por preguiça! Guardarei também os pequenos momentos em que te chateei por causa do confocal, Leonor. Sabes bem que eu recorro logo a ti porque és uma expert. Sara, obrigada por toda a ajuda informática, sabes bem que eu sou uma naba, e tu ajudaste-me imenso a aprender alguns conceitos que necessitarei de usar no futuro.

Bernardo Esteves, Lucas Martins, Pedro Tomás e Alexandre Laborde, obrigado pelas interrupções… e todas as risadas que partilhámos este ano. Alex, vais perder a tua vizinha de bancada este ano, tens menos uma pessoa para chatear! Lucas, obrigado pela ajuda pessoal, agradeço imenso. Bernardo, espero que continues a cantar, tens uma grande voz, e obrigado por partilhares das minhas dores (I cry…).

A todas as pessoas fascinantes que conheci na Fundação Champalimaud, um abraço grande e obrigado por me deixarem participar nesta comunidade tão unida e divertida.

Rita Teodoro, do CEDOC, muito obrigado por todo o apoio que disponibilizaste. Nos momentos mais stressantes estiveste lá para me acalmar e me ajudar. Agradeço-te imenso.

Um grande beijo de obrigado aos meus pais, que sempre me apoiaram em todas as decisões da minha vida. Obrigado por estarem mais uma vez presentes nesta grande etapa. Ao meu irmão, Nuno, obrigado pela força e incentivo. Sei que nunca saberás como pronunciar o meu curso, mas agradeço-te na mesma por me ajudares a finalizá-lo.

Îmi face placere să-i mulțumesc iubitului meu, Răzvan, care a fost în toate momentele din acest an prezent și disponibil să mă ajute. Ajutorul tău a fost extraordinar, nu reușiam sa termin acest an fără tine. La socri mei Gabriela și Iulian, pentru a fi disponibil să mă ajute în timp ce eram singură și lucram. În totdeauna a fost mâncare pentru mine în zilele care eram singură și nu făceam mâncare pentru mine. Mulțumesc mult.

Financial Support

All the required financial support in order to perform all experimental and complementary work for the project entitled “Mapping corticostriatal synapses onto spiny projection neurons” was provided by the Neurobiology of Action Lab, using funds from internal (Champalimaud Foundation) and external (Fundação para a Ciência e Tecnologia and European Union) sources.

Fundação Champalimaud

Abstract

Imaging methods for visualizing synaptic contacts within neuronal circuits are under constant development and could contribute to the generation of a connectome of the striatum, which will be crucial to decode how striatal cells integrate motor information[1–4]. We attempted to optimize the mammalian GFP reconstitution across synaptic partners (mGRASP) technique to better understand how spiny projection neurons (SPNs) integrate input information from cortical intratelencephalic (IT) and pyramidal tract (PT) neurons. In order to do that, we set out to map corticostriatal inputs to SPNs with mGRASP and study their density and distribution at the single cell level. We used adeno associated viruses (AAVs) to express the pre and postsynaptic forms of split-GFP (pre- and post-mGRASP, respectively) in the motor cortex and dorsolateral striatum (DLS), in order to detect synaptic contacts as the loci of GFP reconstitution across the synaptic cleft. However, we were unable to identify a GFP reconstitution signal that was strong and frequent enough to be distinct from unspecific puncta-like fluorescence in the slice. We tested protocols aimed at reducing the non-specific signal, which were not successful. We then tried to amplify the specific mGRASP signal using anti-GFP antibodies. Despite two of the three antibodies tested had previously been reported as specific towards reconstituted GFP, we found that they also recognized either pre-mGRASP, or both pre and post-mGRASP isoforms, in our system. While this enabled us to confirm the correct expression of the pre and post-split-GFP isoforms in cortical and striatal neurons, respectively, it prevented the amplification of the reconstituted GFP specific signal and the subsequent analysis of corticostriatal connectivity. Nonetheless, we were able to optimize a neuronal reconstruction methodology, which will be useful for future analysis of input distribution by mGRASP or other techniques. This methodology was tested in striatal SPNs and cholinergic interneurons (ChIs) and it showed clear morphological distinctions between the dendritic distribution of these two neuronal types. Future efforts could focus on the continued quest for a successful protocol to amplify the mGRASP signal or to use classical immunostaining methods for synapse identification. Either of these methods could be combined with functional analysis and the neuronal reconstruction methodology to map corticostriatal input distribution along SPN and ChI dendritic trees.

Resumo

Metodologias à base da microscopia ótica para a visualização de sinapses ao longo de circuitos neuronais estão em constante desenvolvimento, podendo contribuir para a geração de um conectoma do estriado que será essencial para descodificar como as células desta região do cérebro integram informação motora[1–4]. Tentámos otimizar a técnica "*mammalian GFP reconstitution across synaptic partners (mGRASP)*" para entender melhor como é que os neurónios médios do estriado (*spiny projection neurons, SPNs*) integram a informação vinda das projeções dos neurónios corticais intratelencefálicos (IT) e piramidais (PT). Com esse propósito, procurámos mapear os contactos sinápticos cortico-estriatais com *mGRASP* e estudar a sua densidade e distribuição a nível celular. Usámos partículas adenovirais (AAVs) para expressar as duas partes complementares da GFP, a forma pré-sináptica e pós-sináptica (denominadas pre- e pos-mGRASP, respetivamente) no córtex motor e na região dorsolateral do estriado (DLS), para detetar os contactos sinápticos através da reconstituição da molécula de GFP através da fenda sináptica. No entanto, não fomos capazes de identificar nenhum sinal relativo à reconstituição da GFP que fosse forte e frequente o suficiente para se distinguir de outros sinais inespecíficos nas fatias de cérebro analisadas. Testámos outros protocolos, com o intuito de reduzir o sinal inespecífico, mas não foram bem sucedidos. Tentámos então amplificar o sinal específico do *mGRASP* usando alguns anticorpos anti-GFP. Apesar de dois dos três anticorpos testados já terem sido descritos como sendo específicos para a forma reconstituída da GFP, descobrimos que reconheciam ambas as isoformas pre- e post-mGRASP ou só a pre-mGRASP, no sistema testado. Embora estes resultados nos tenham permitido a confirmação da expressão correta de ambas as isoformas complementares da GFP nos neurónios corticais e do estriado, não permitiu a amplificação do sinal específico referente à reconstituição da GFP e a posterior análise da conectividade cortico-estriatal. Todavia, fomos capazes de otimizar um método de reconstrução neuronal, que pode vir a ser útil para futuras análises da distribuição sináptica com *mGRASP* ou outras técnicas. Esta metodologia foi testada em neurónios médios do estriado e interneurónios colinérgicos, e demostrou uma distinção morfológica clara entre a distribuição dendrítica destes dois tipos de neurónios. Estudos futuros podem continuar a procura de um protocolo para amplificar eficientemente o sinal específico do *mGRASP* ou usar protocolos clássicos de imunohistoquímica para identificar estas sinapses. Qualquer uma destas estratégias pode posteriormente ser combinada com análises funcionais e reconstruções neuronais para mapear os contactos sinápticos cortico-estriatais ao longo das arborizações dendríticas dos neurónios médios e colinérgicos do corpo estriado.

Index

Introduction

- Cortex-basal ganglia loops encode motor information

Motor actions depend on the coordinated activity of organized networks between the cortex, thalamus and basal ganglia (BG)[5,6]. The BG are comprised of intertwined subcortical nuclei that receive excitatory input, mainly from the cortex and the thalamus[7]. The central nucleus of these ganglia is the striatum, as it integrates, computes and outputs motor-related information. The striatum has been divided into three functional areas, dorsolateral, dorsomedial and ventral, based on different input sources, and a posterior region has recently been described[8]. The connectivity between the cortex and the striatum is directional and monosynaptic. Therefore, the striatum only connects indirectly with the cortex through downstream circuits[9]. There are two important pathways that segregate in the striatum to deliver motor information downstream: the direct and indirect pathways. Through these pathways, a collection of information is delivered to the output nuclei of the BG. The BG, ultimately, modulate the activity of the thalamus. The thalamus projects back to the cortex and striatum through excitatory fibres, therefore, closing the loop. This feedback loop is thought to support learning and habit formation[9,10] by refining cortical network activity.

The cortex is a crucial structure for action planning[11–13]. The motor cortex is the primary input source to the dorsolateral striatum[6]. Corticostriatal neurons are glutamatergic and project their excitatory axons ipsilaterally and/or contralaterally, as detailed in the following section. Besides the primary motor cortex (M1), other areas also convey information that could contribute with motor information such as the premotor cortex and the supplementary motor cortex[14,15]. While the motor cortex is one of the most important motor inputs, the thalamus is also essential for controlling voluntary movement through the BG circuitry[16,17]. The thalamus contributes with a third of all excitatory synapses to the striatum[1], and it connects to both the direct and indirect pathways, in similarity to cortical afferents[7,18]. The main sources of axonal projections from the thalamus to the dorsal striatum are the Centrolateral/Paracentral and Parafascicular thalamic nuclei[1]. Thalamostriatal neurons and corticostriatal neurons project to the same subregions of the striatum[6,8]. Thus, the thalamus is closely coordinated with the cortex and the striatum during motor information processing.

The striatum has a large population of spiny projection neurons (SPNs; also called medium spiny neurons), which are inhibitory neurons that express the gamma-aminobutyric acid (GABA) neurotransmitter and comprise over 90% of all striatal neurons[19]. SPNs are the major output neurons as well as the major input target of the striatum[6]. Therefore, these cells provide substrate for specific information processing operations[20]. In addition, there is a small population of cholinergic interneurons (ChI) distributed within the striatum that also receive

excitatory input from the cortex and thalamus[17,21–23]. ChI release acetylcholine, which can modulate SPN activity[24].

SPNs segregate into dopamine D1-receptor expressing (D1-SPNs) and D2-receptor expressing SPNs (D2-SPNs). D1- and D2-SPNs are homogenously distributed across the striatum and have different synaptic targets: D1-SPNs project to the internal globus pallidus (GPi) and to the substantia nigra pars reticulata (SNr), with minor collaterals to the external segment of the globus pallidus (GPe), comprising the direct or striatonigral pathway (Figure 1); D2-SPNs convey the information to the SNr via the GPe and the subthalamic nucleus (STN). As a result, the D2-SPN pathway is termed the striatopallidal or indirect pathway[6,9](Figure 1). In the direct pathway, there are two GABAergic synapses between the striatum and the thalamus, thus, activation of the direct pathway causes a disinhibition of excitatory inputs from the thalamus to the motor cortex. On the other hand, STN projections are excitatory, therefore, activation of the indirect pathway results in the activation of STN neurons that activate SNr cells to inhibit thalamocortical projection neurons (Figure 1). As a result, cortical and striatal activity are modulated by thalamic feedback afferents[6,18,25].

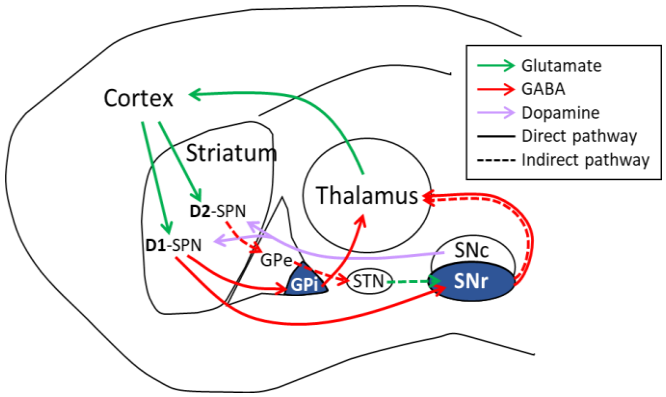

Figure 1 – A simplified representation of a motor circuit in a sagittal overview. Only the main pathways and dopaminergic innervation from the SNc (and not the ventral tegmental area, for simplicity) are represented. Red arrows represent inhibitory or GABAergic connections; green arrows depict excitatory connections; Blue filled structures indicate the main output nuclei of the basal ganglia. *GPe- external segment of the globus pallidus; GPi- internal segment of the globus pallidus; SNr - substantia nigra pars reticulata; SNc - substantia nigra pars compacta; STN - subthalamic nucleus.*

Regarding motor control, D1- and D2-SPNs were initially suggested to play opposite roles. Activation of the direct pathway would disinhibit the thalamus, that would, therefore, lead to cortical excitation and facilitate movement – the 'GO' signal[22,26–28]. On the other hand, the activation of the indirect pathway would inhibit the thalamus, reducing cortical excitation and resulting in the inhibition of movement – the 'NO GO' signal[22,26–28]. The simplicity of the proposed 'GO'/'NO-GO' model allowed a direct interpretation of the role of these pathways on motor function and motor disorders[29–31,22]. However, recent evidence challenged this model by showing that D1- and D2-SPN activation is concurrent, complementary and

necessary for movement[32–35], assembling into functional clusters during action performance[34,36,37]. Hence, the functional roles of the direct and indirect pathways are still a matter of debate.

In addition to the glutamatergic thalamic- and corticostriatal inputs, the striatum receives dopaminergic innervation, which regulates striatal neuronal activity[38]. Dopamine plays a critical role in the regulation of the direct and indirect pathway by modulating, for example, SPN firing activity[25,38–41]. Dopamine fibres that synapse in the striatum arise from the ventral tegmental area, substantia nigra pars compacta (SNc) and the retrorubral field. Moreover, dopamine activates different signalling cascades in D1- and D2-SPNs, as D1 and D2 receptors are G-protein coupled receptors positively and negatively coupled to adenylate cyclase and PKA production, respectively. Ultimately, D2 receptor activation by dopamine leads to the inhibition of D2-SPN activity, while on D1-SPNs leads to spiking activity facilitation[6,22,25,38]. Along these lines, dopamine release in the dorsal striatum is believed to facilitate movement by activating the direct pathway and inhibiting the indirect pathway[25,41]. Dopamine's role in movement is evidenced in Parkinson's disease, where midbrain dopaminergic neuronal cell death greatly reduces striatal dopaminergic innervation[6,10,25,42]. This loss of dopamine causes overactivation of the indirect pathway and is associated with parkinsonian motor symptoms, such as difficulties in movement initiation[10,22,31,43,44].

- Corticostriatal projection neurons

The cortex is structured into six laminar layers along the transversal plane. Each layer contains pyramidal neurons with local and/or long-range patterns, that differ from one another. While long-range projecting neurons in Layer (L) 2/3 are mainly corticocortical, neurons in L5, and to a lesser extent in L6, have corticocortical and/or corticostriatal projections[9,22,45,46]. Corticostriatal neurons release glutamate as a neurotransmitter and provide the major source of excitatory input to striatum[45,47]. There are two main types of corticostriatal neurons: intratelencephalic (IT) and pyramidal tract (PT) neurons[22,48] (Figure 2A). These populations have different laminar position and synaptic targets. Their projection patterns diverge within the cortex but also in subcortical areas[22,46,48,49]. IT neurons are widely distributed across L2-L6 and project ipsi- and contralaterally, through the *corpus callosum*, to other cortical areas and the striatum[22,46,50]. PT neurons are concentrated in L5B and project to subcortical regions such as the BG, thalamus and brainstem[22,49,50]. Moreover, PT projections do not cross the *corpus callosum*, projecting only from the cortex to the ipsilateral striatum[6,51]. Consequently, the striatum is the only subcortical structure where inputs from both IT and PT neurons converge (Figure 2B).

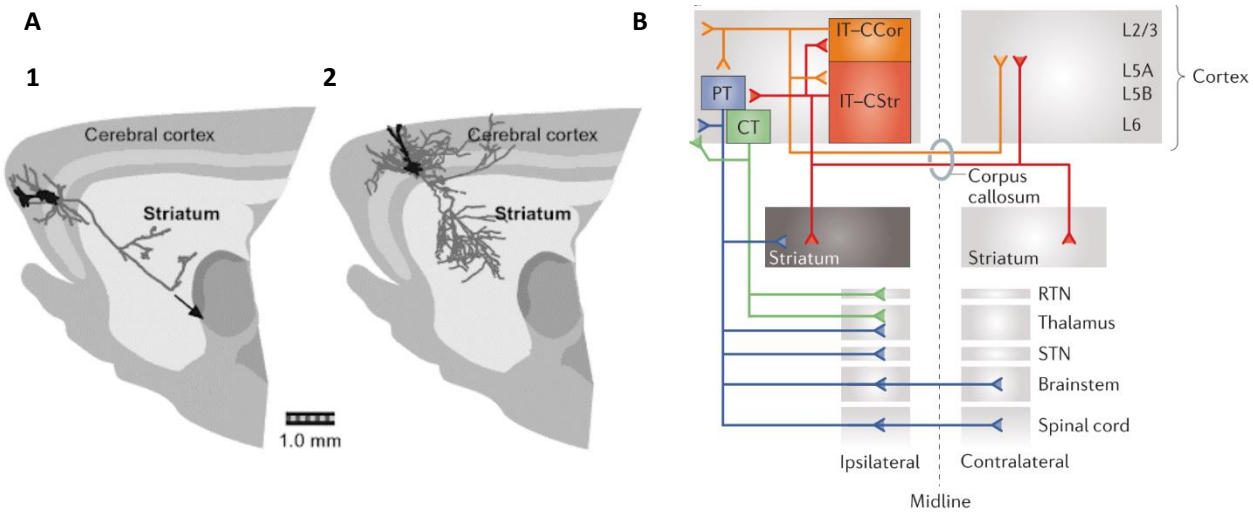

Figure 2 – Pyramidal tract and Intratelencephalic neurons projection patterns and synaptic partners. A, Tracings of dendrites (black) and striatal axons (grey) of the two subtypes of corticostriatal neurons: 1- Pyramidal Tract (PT); 2- Intratelencephalic (IT) adapted from: Gerfen and Bolam, 2010[6]. B, A simplified representation of the long-range projections of corticostriatal (CStr) and corticocortical (CCor) neurons. The striatum receives input from both PT and IT neurons. *CT - Corticothalamic neurons, RTN -Reticular thalamic nucleus, STN – Subthalamic nucleus.* Adapted from: Shepherd, 2013[9].

Locally, L5 corticostriatal neurons are hierarchically organized. IT neurons connect to other IT and to PT neurons. On the other hand, PT neurons connect to other PT but do not synapse onto IT cells. So, in the cortical local circuit, IT neurons control PT activity while PT neurons cannot directly affect IT cells. Both IT and PT neurons synapse onto D1-SPNs, D2-SPNs and interneurons in the striatum[22,23,52,53].

Cortical projections to the striatum are stereotypical. IT neurons have a considerable axonal overlap and a stereotyped and extended arborization in the ipsilateral striatum[54]. PT neurons have more local projections, with less overlap[9,55], which may represent a useful sub-circuit strategy for basal ganglia loops, as these neurons may integrate more specific information (Figure 2A)[3,6,56]. Moreover, corticostriatal axons from individual neurons are widely distributed so that they synapse with as many SPNs as possible while making a minimal number of contacts with each postsynaptic neuron[6,45,57]. The probability of neighbouring SPNs having common cortical inputs is very low, generally less than 100 inputs [40,57,58]. This suggests that, if the firing threshold is 100 inputs or above, activation of an arbitrary group of 100 inputs to a given cell could fire that cell without firing others, due to their low input overlap. Therefore, the topology of corticostriatal connections appears to be limited by the access of cortical cells to SPNs, leading to the proposal of the "combinatorial selection model", where an effective combination of cortical inputs is highly selective for a particular SPN[40,57].

However, the connections between IT and PT-neurons with D1-and D2-SPNs remain to be fully understood as different methodologies reach different results[6,9,52,59]. It was initially proposed that IT neurons could specifically synapse on D1-SPNs while PT neurons could contact only D2-SPNs, based on the following observations. Using retrograde labelling, the anatomic analysis of synaptic contacts by electron microscopy and light microscopy revealed a significant bias of IT neurons towards D1-SPNs and PT neurons towards D2-SPNs[60]. Moreover, regarding the electrical properties of SPNs, D2-type neurons are more prone to respond to low stimulation intensities[61]. The D2 lower threshold for spiking was hypothesized to rely on larger axospinous terminals. As PT-neurons are more inclined to have larger terminals and appear to target larger spines[46,50,60], it was suggested that D2-neurons could have greater PT innervation[61] (Figure 3A).

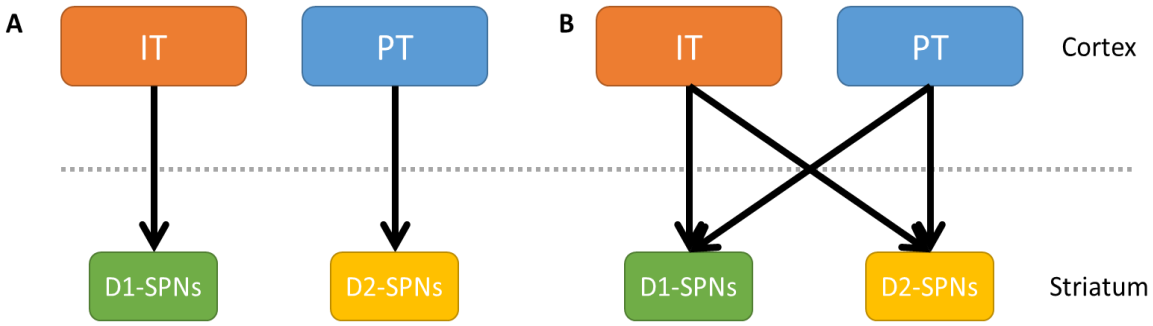

Figure 3– Schematic representation of the different corticostriatal projections from IT (Intratelencephalic)- and PT (Pyramidal tract)-neurons onto D1- and D2-expressing neurons in the striatum. A, Model based on the anatomical data (Morita, 2014[59]). B, Model based on electrophysiological recordings followed by optogenetic activation (Kress et al, 2013[52]).

Optogenetic approaches allowed new strategies to survey the responsiveness of single SPNs. Kress et al. employed optogenetic activation of either PT or IT axons projecting onto SPNs and failed to find any differences between the PT or IT cortical inputs onto D1- or D2-SPNs[52]. This finding highlighted that both IT and PT neurons strongly innervate both SPNs. Nevertheless, Morita et. al. suggested that synapses might show a negligible response to a single spike but have stronger responses after several spikes, which would mean that the anatomical bias would not be evident after the first optogenetic stimulation, but rather after repeated stimulation[59].

- Spiny Projection Neurons

Spiny projection neurons (SPNs) are the principal cells of the striatum and are classified as D1- and D2-SPNs according to the expression of different dopamine receptors, as detailed in the first section of the introduction. These two cell types also exhibit other distinctions in

molecular composition: D2-SPNs express enkephalin while D1-SPNs express substance P and dynorphin [6,44,62]. In spite of differences at the biochemical level, D1- and D2-SPNs are rather similar in their electrical and physiological properties[20]. However, it is not known whether the distribution of corticostriatal inputs differs between D1- and D2-SPNs[52,59]. A differential number and location of different types of cortical inputs would likely affect the integration and computation of cortical information by SPNs.

Anatomically, SPNs have a cell body of 9-15µm in diameter[63]. The dendritic tree is formed by 5 or 6 primary dendrites which radiate and divide once or twice within a spherical volume of 250-500µm in diameter[20,63] (Figure 4A). D1-SPNs have a greater total dendritic length and more branches than D2-SPNs, due to a different number of primary dendrites[63]. SPNs have one main axon originating from the cell body that projects to target areas. Each SPN also sends out local axon collaterals, which divide multiple times and form an extended network that overlaps with dendritic trees of nearby neurons (Figure 4B)[20].

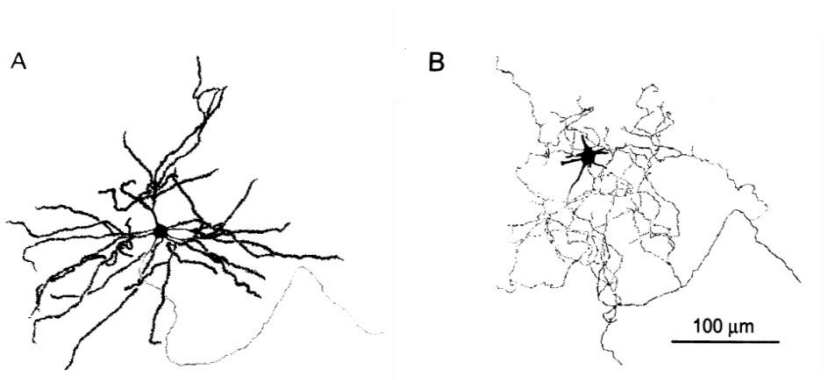

Figure 4 – Reconstruction of a spiny projection neuron. A, Dendritic arborisation, B, Local axonal collaterals of an SPN. Adapted from: Plenz and Wickens, 2010[20].

SPNs exhibit an inward potassium (K^+) current that maintains the membrane potential in a hyperpolarized state[22,64]. However, SPN membrane potential transitions between a hyperpolarized state near the K^+ equilibrium (Down state) to a more depolarized state near the spike threshold (Up state)[20,63,65]. The depolarized state is also named "prepared state" because it facilitates action potentials [39,66]. The membrane potential shift to an Up state was suggested to depend on the synchronized excitation of a great number of pre-synaptic neurons. On the other hand, depolarization events that resemble Up-states can be elicited in SPNs in response to synchronized activation of a small number of neighbouring distal dendritic spines[39,64,66]. As the connectivity between cortical afferents and individual SPNs is sparse, this local synchronized activation of a few inputs could be an alternative manner to reach an Up state and/or cell firing, rather than the simultaneous activation of a large number of cortical presynaptic neurons[39].

SPNs receive excitatory inputs mainly from the cortex and the thalamus, which synapse preferentially at dendritic spines, rather than the shaft[18,60,67]. Most inputs from midbrain dopamine neurons also target dendritic spines[6,68]. However, while corticostriatal and thalamocortical terminals synapse on spine heads, dopaminergic boutons contact the necks of spines that normally also contain a glutamatergic synaptic connection at the head[6,68]. On the other hand, inhibitory synapses from other SPNs and striatal GABAergic interneurons, as well as striatal cholinergic interneurons, are generally localized in dendritic shafts and cell bodies[6,69] (Figure 5). Besides the spine input differential targeting, there is also a preferential input distribution for presynaptic terminals in regards to their distance to the cell body: inputs from cortical, thalamic and midbrain dopaminergic neurons target distal fractions of the dendritic branches, while cholinergic (ChAT) and a subset of GABAergic interneurons target proximal dendritic spines and cell bodies[6,70–72]. This is a shared characteristic between D1- and D2-SPNs[6,72](Figure 5).

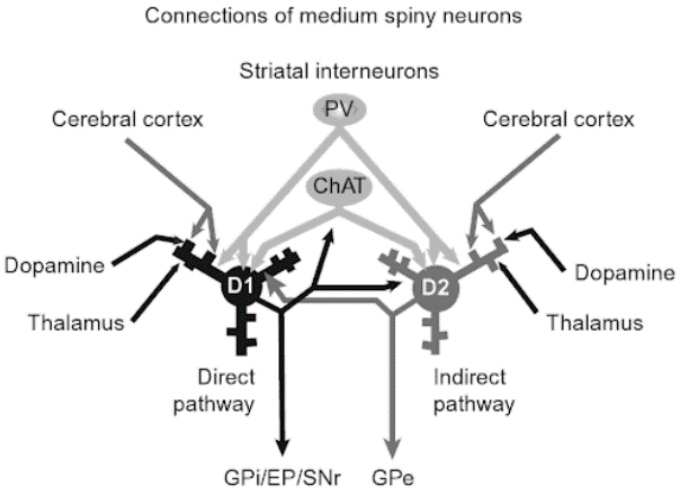

Figure 5– Diagram of inputs to distal and proximal dendritic areas of SPNs. Cortical, thalamic and dopaminergic inputs preferentially target distal dendritic spines while a subset of GABAergic neurons expressing the Ca^{2+}–binding protein parvalbumin (PV) and cholinergic (ChAT) interneurons target proximal dendritic areas and cell bodies. Adapted from: Grefen and Bolam, 2010[6]. *D1 – D1-SPNs, D2 – D2-SPNS, GPi – Globus pallidus internal segment, EP -Entopeduncular nucleus, SNr – Substancia nigra reticulata, GPe – Globus pallidus external segment.*

Altogether, SPNs display anatomical strategies to differentially weight specific inputs. Therefore, the integration of thalamic and IT or PT cortical information by SPNs will be dependent on the anatomical distribution of these inputs along their dendritic tree.

- Cholinergic interneurons in the striatum

There are other neuronal types in the striatum besides the dominating SPNs. These interneurons do not project outside the striatum. Instead, they are distributed within this structure and make synaptic contacts with SPNs, modulating striatal output. Interneurons could be divided into GABAergic and Cholinergic interneurons (ChIs), based on the neurotransmitter they release[73]. ChIs release acetylcholine (Ach) and choline acetyltransferase (ChAT), which is a specific marker for these cells[74], summing up to 2% of the striatal volume[19,74].

Functionally, ChIs respond to sensory stimuli and their spiking activity increases during changes in the networks' input[23,24]. Their input can come from cortical and/or thalamic afferents[17,21–23]. As opposed to SPNs, ChIs are tonically active *in vivo* and comprise highly dense dendritic arborizations with low spine density[22,75,76]. Morphologically, these neurons have a large soma, 2-4 large primary dendrites that bifurcate over a range of 1 mm and an extensive axon[74]. Moreover, ChIs cluster into functional domains. The most abundant ChI domain is around the anterior dorsal striatum[4].

ChI synaptic innervation is very heterogeneous, receiving symmetric and asymmetric inputs from various sources. About 60% of ChI's inputs are GABAergic, 20% are glutamatergic and the remaining is still unknown (Figure 6)[77]. About 24% of synaptic inputs to ChIs are from SPNs. But ChIs also connect to SPNs in their dendritic spines and shafts[77], modulating their firing rate and neurotransmitter release[6,23,78]. By these means, ChIs are proposed to act as additional cellular substrates for synaptic cross-talks between SPNs[38,41]. In addition, ChIs are innervated by midbrain dopaminergic neurons[78] (Figure 6), and acetylcholine can also as act as a neuromodulator on dopaminergic, glutamatergic presynaptic terminals and on SPN dendritic spines[76,78]. Therefore, both ACh and dopamine represent important regulators of SPNs activity and striatal function[79].

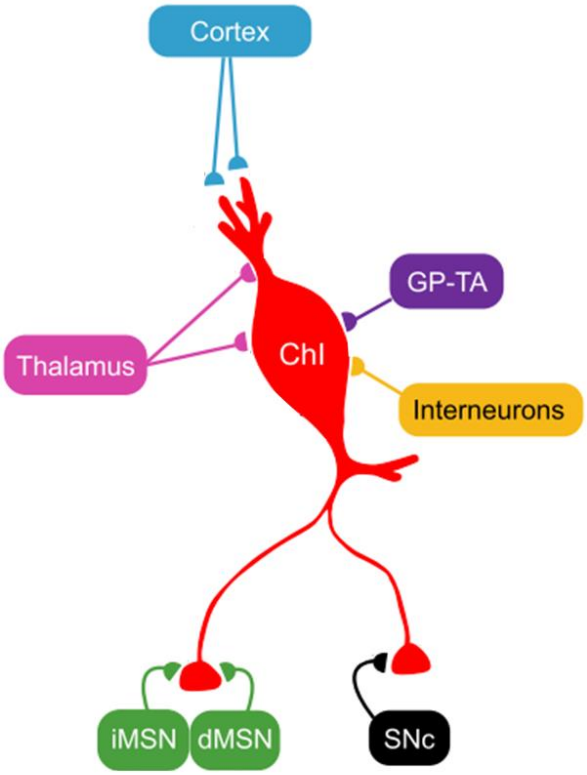

Figure 6 – Schematic representation of inputs to a cholinergic neuron (ChI) in the striatum. Adapted from: Abudukeyoumu et al, 2019[24]. *iMSN – indirect pathway medium spiny neuron (D2-SPN), dMSN – direct pathway medium spiny neuron (D1-SPN), SNc – Substancia nigra pars compacta, GP-TA - arkypallidal- type A GABAergic afferents from globus pallidus.*

- Mammalian GRASP mapping of synaptic contacts

Functional connectomes of complex neural circuits are crucial to understand brain function and behaviour[80,81]. Decoding brain activity strongly depends on the anatomical constrains of each brain area and cell type. Therefore, different technologies were developed to provide high-resolution mapping at the synapse level. While light microscopy and fluorescent-based approaches have recently benefitted from technical advances to improve resolution[82], electron microscopy still offers the highest resolution to characterize synapses at the molecular level. Nevertheless, electron microscopy is laborious and is only practical for small volumes[83]. Recently, new fluorescent-based methods have been developed to engineer alternative approaches for circuit mapping that allow the usage of light microscopy, such as array tomography, Brainbow techniques, trans-synaptic tracing and green fluorescent protein (GFP) reconstitution across synaptic partners (GRASP). All of the methods mentioned enable single synapse imaging by tracing small clusters of neurons with different fluorophores[2,81,84,85].

GRASP was first designed in *Caenorhabditis elegans*[86] and it was later applied to *Drosophila melanogaster*[87] and to mammalian systems[80,81,88]. It is based on the complementary reconstitution of GFP from two split-GFP fragments called GFP1-10 and GFP11[86]. At a protein level, GFP1-10 contains the first 214 residues of stable GFP, while GFP11 only contains 16 residues[89]. Each split GFP is also soluble, inert and non-fluorescent in the absence of their complementary isoform[86,90]. These molecules are expressed separately in two different neuronal populations fused with membrane proteins that localize them to the synaptic cleft (Figure 7). When the two different split-GFPs are tethered to opposite synaptic membranes, the GFP is reconstituted and the pair recovers its fluorescence by reconstituting the chromophore[90], as illustrated in Figure 8A. In mammalian GRASP (mGRASP), the design of each split-GFP considered the reconstitution over synaptic clefts in the mouse brain (~20 nm) ensuring reconstitution specifically at synapses and preventing non-specific signals[81].

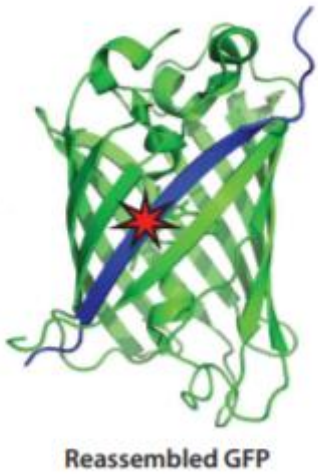

Figure 7 – Illustration of the 3D structure of the Reconstituted GFP signal through mGRASP. Blue represents split GFP11 and green represents split GFP1-10. Adapted from: Kent et al, 2008[91].

The mGRASP constructs can be delivered using viral strategies that include the Cre-recombinase system. To avoid co-expression in the same neuronal population, Cre-dependent 'switch on' and 'switch off' versions for pre- and post-mGRASP are available. When Cre-recombinase is present, the construct is flipped within the two LoxP sites, turning it either ON or OFF, respectively (Figure 8B). Thus, neuronal specificity can be reached by taking advantage of Cre transgenic mouse lines or Cre-expressing adeno-associated viruses (AAVs). Moreover, gene-delivery strategies can address signal sparseness within the brain area being mapped[81].

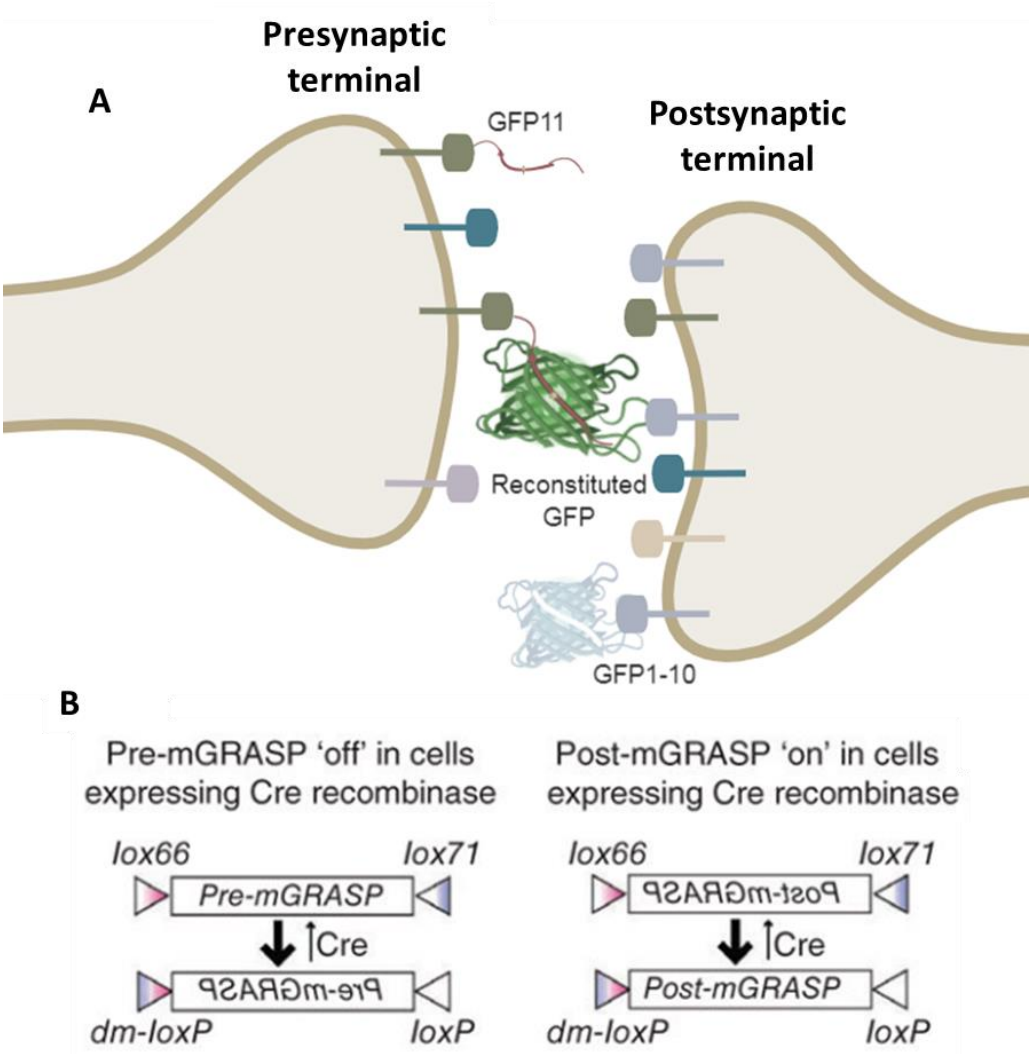

Figure 8 – Schematic representation of synaptic mGRASP components. A – Schematic reconstitution of fluorescent GFP. B – Cre recombinase-dependent 'switch on' and 'switch off', applied to pre-mGRASP and post-mGRASP constructs, respectively. Adapted from: Kim et al, 2012[81]. Images from http://BioRender.com, Kent et al, 2008[91] and Romei et al, 2019[90].

To allow the visualization of pre-mGRASP distribution and identification of the presynaptic neuron, fluorescent monomeric Cerulean (mCerulean) was fused to the pre-mGRASP construct containing split GFP11 (Figure 9 top). Additionally, mCherry tagged with a nuclear localization sequence was also fused to the cytosolic end of the construct via the self-cleavable 2A peptide, in order to label the nuclei of presynaptic neurons expressing mGRASP. On the other hand, dimeric Tomato (dTomato) was fused also via 2A peptide to the cytosolic end of the post-mGRASP construct containing split GFP1-10, to allow visualization of the postsynaptic neurons (Figure 9 bottom)[81].

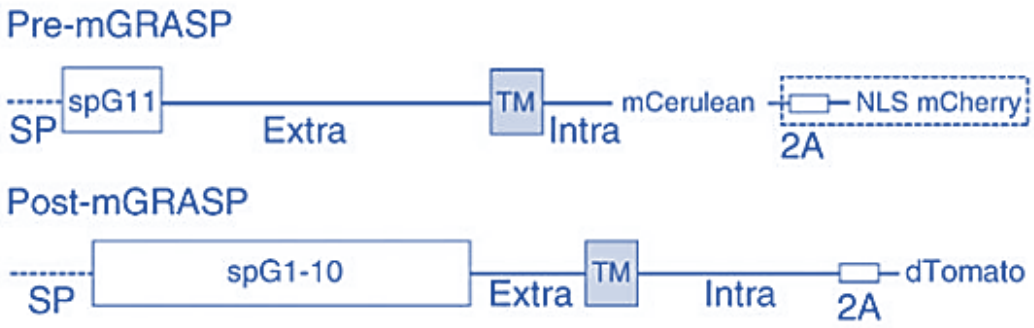

Figure 9 – Representation of pre- and post-mGRASP designed by Kim et al. (2013) composed of signal peptide (SP; which allows proteins to be secreted via Golgi apparatus, in this case to be inserted in the membrane), split-GFP fragment GFP1-10 (spG1-10) or GFP11 (spG11), extracellular domain (Extra), transmembrane domain (TM) and intracellular domain (Intra) followed by mCerulean, 2A-NLS-mCherry or 2A-dTomato to identify neuronal processes or nuclei. Adapted from: Kim et al. 2013[80].

Since mGRASP can be employed in both local and long-range functional circuit mapping[81], it is a good method to approach corticostriatal synaptic connections onto SPNs, and more specifically, IT and PT cortical inputs to D1- and D2-SPNs, thus providing a connectivity map of the main circuitry of the basal ganglia.

Objectives

Corticostriatal synapses are the main excitatory gate where motor information is transmitted to spiny projection neurons (SPNs) in the striatum. Changes in the input weight can greatly affect how information is processed and integrated by these cells. However, the distribution and density of different cortical inputs to the two main SPN populations remains understudied.

The main goal of this project is to map corticostriatal inputs from intratelencephalic (IT) and pyramidal tract (PT) neurons to striatal SPNs to better understand how striatal neurons sample and integrate motor information from the cortex.

To achieve this goal, we devised the following experimental aims:

- To set up the mGRASP labelling technique in corticostriatal synapses and its associated digital tools for synaptic analysis.

- To study the spatial pattern of IT/PT inputs to D1- and D2-SPNs, analyzing their location (e.g. distal vs proximal dendritic locations) and potential distribution biases (synaptic clustering vs random distribution) within the postsynaptic dendritic tree.

- To characterize the type, average size and number of corticostriatal (IT and PT) synapses onto D1- and D2-SPNs.

Methods

1. Experimental animals

All animal procedures were conducted in accordance with protocols approved by Direção Geral de Alimentação e Veterinária (DGAV), the Rodent Facility of the Champalimaud Foundation, Lisbon, Portugal and the Ethical Committee at NOVA medical School, Lisbon, Portugal. Adult mice between 2-3 months of age from different transgenic lines were used for surgery. The animals were housed on a 12-hr light/dark cycle at 23ºC with *ad libitum* access to food and water.

Experiments were conducted in IT-CRE (Tlx3 mouse line: STOCK Tg(Tlx3-cre)PL56Gsat/Mmucd), PT-CRE (OE25 line: STOCK Tg(Chrna2-cre)OE25Gsat/Mmucd) and D1-CRE (EY217 line: Tg(Drd1a-cre)EY217Gsat/Mmucd) mice. These transgenic animals were originally obtained from The Jackson Laboratory and were backcrossed to C57BJ/6J background for at least 6 generations. All mouse lines were subsequently maintained at the Champalimaud Foundation animal facility. Additional information regarding mouse strains are indicated on Annex I

2. Stereotaxic surgery for viral injection

Adeno-associated viruses (AAVs) were delivered by stereotaxic brain surgery[80,92]. Under sterile conditions, each mouse was anesthetized in an induction chamber with isoflurane 5% at 1-1.5 l/min until the toe-pinch reflex (a muscular response to applied pressure) elapsed. Mice were then placed onto a stereotaxic frame (David Kopf Instruments, Model 962LS) on top of a heating pad (ATC1000, World Precision Instruments) kept at 37ºC. Throughout the surgery, isoflurane was continuously administered through a breathing mask at 1-2% at 1-1.5 l/min. Eyes were kept moist with eye gel (Visidic gel). Then, the head was shaved and cleaned with 70% ethanol and iodine. The skull was exposed with an incision through the midline allowing Bregma and Lambda identification (Figure 10). The head was horizontally aligned, and a small hole was drilled (Henry Schein, tungsten drills #1/4) on the injection site. All coordinates were estimated from the Allen Mouse Brain Atlas. AAVs were injected in both motor cortex M1 region (coordinates: AP=+0.8mm and ML=±1.6mm in relation to bregma and, DV=-0.75mm from the surface of the skull) and DLS (AP=+0.8mm, ML=±2.3mm, DV=-2.3mm), either unilaterally into the right side or bilaterally with M1 and DLS injections contralateral to one another. A Nanoject II Injector (Drummond Scientific) was used at a rate of 4.6 nl per pulse every 5 s. AAV were injected using sharp pipettes pulled from glass

capillaries (Drummond 3.5'' capillary tubes #3-000-203-G/X)) in a vertical puller (Narishige PC-10 Dual Stage) and bevelled to facilitate the penetration through the dura. These conditions were optimized to allow high cortical expression in L5, abundant projection afferents to DLS and high expression in DLS. To minimize backflow of the AAV solution, the pipette was withdrawn after 5-10min from the last pulse. The skin was then sutured and/or glued with Vetbond tissue adhesive (3M). Carprofen mouse mix (analgesic and anti-inflammatory with 0.3ml Rimadyl in 9.7 ml saline) was administered subcutaneously at 100-200 ul/ 20-30g Body weight (BW). Mice were left to recover at 37ºC and placed back on their home cage when they regained conscience. The wound was monitored for at least 1-2-day post-surgery to ensure no infections/re-openings of the skin.

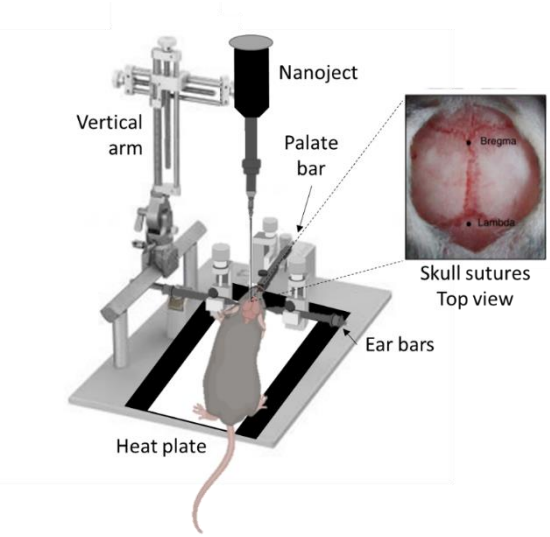

Figure 10 – Schematic representation of the stereotaxic apparatus for AAV injection *in vivo*. The stereotaxic reference points are represented on the right – Bregma is the anterior joint between the frontal bone and temporal lobes while Lambda is the posterior joint, separating the occipital bones. Adapted from: Feng et al, 2014[80].

3. Experimental approach for gene delivery

Depending on the strategy, one or more of the following AAVs expressing mGRASP were used (Table 1)[81] (all constructs are from Addgene, www.addgene.org). Virus production was performed at the Champalimaud Foundation by the Molecular and Transgenic Tools Platform.

Table 1- mGRASP variants, from: Kim et al, 2012[81] and Feng et al, 2014[80]. *gc/ml - genome copies per millilitre, Coexp - coexpression; d.f. - directly fused CAG -promoter designed from cytomegalovirus promoter early enhancer element*[93].

	AAVs							
Class	Full name	Short name	Addgene ID	Cre dependence	mGRASP (1st gene)	Coexp. link	Colour protein (2nd gene)	Titter
Presynaptic mGRASP	AAV-CAG-Jx-OFF-pre- mGRASP-mCerulean	CreOFFPre	51900	OFF	GFP11	d.f.	mCerulean	3,09x10^{13} gc/ml
	AAV-CAG-pre-mGRASP-mCerulean-2A-nls-mCherry	Pre-mGRASP	34911	No	GFP11	2A	mCherry	1,58x10^{13} gc/ml
Postsynaptic mGRASP	AAV-CAG-Jx-ON-post- mGRASP-2A-dTomato	CreONPost	34913	ON	GFP1-10	2A	dTomato	2,35x10^{13} gc/ml

The AAV2-CMV-PI-Cre-rBG (AAV-Cre; titter 4.648x10e12 gc/ml) was used to induce mGRASP expression. On the first approach we aimed to specifically label IT or PT neurons with pre-mGRASP and sparsely label SPNs with post-mGRASP (no distinction between D1- or D2-SPNs). Therefore, we injected IT-*CRE* and PT-*CRE* mice with CreOFFPre in M1 (AP=+0.8mm; ML=±1.6mm and DV=-0.75mm) while a 4:1 mix of CreONPost to AVV-Cre was injected in the DLS (AP=+0.8mm; ML=±2.3mm and DV=-2mm or -2.3mm). The AAV-Cre suspension was diluted in PBS to either 1:10, 1:300, 1:500, 1:1700, 1:1000 or 1:10000. As a second approach, we aimed to label cortical neurons with pre-mGRASP and specifically label D1-SPNs with post-mGRASP in the contralateral side. This enabled the interrogation of IT cortical neuron inputs to contralateral D1-SPNs (as IT neurons, unlike PT neurons, project to the contralateral striatum). Therefore, we injected D1-Cre mice with Pre-mGRASP in M1 at AP=+0.8mm, ML=±1.6 and DV=-0.75mm and CreONPost in the DLS at AP=+0.8mm, ML=±2.3mm and DV=-2 or -2.3mm.

4. Mouse perfusion and brain slice preparation

After 2-4 weeks post-surgery, mice were injected intraperitoneally with a ketamine/xylazine mix (120mg/KgBW Ketamine, 16mg/KgBW Xylazine, 1.2ml Imalgene 1000, 0.8ml 2% Rompun and 8ml saline) at 0.1 ml/10 g BW. When the toe-pinch reflex was lost, mice were placed on top of an agar plate and pinned on the paws. A cut was made posterior to anterior around the diaphragm. Afterwards, the diaphragm was opened, and the bottom ribs were cut and folded backwards. A small 25mm calibre needle (23G), connected to the perfusion tubing, was then inserted in the left ventricle. After the right atrium was cut, a motorized pump was turned on to start perfusing PBS. As soon as the liver turned 'whitish' – meaning that the

blood was replaced by PBS – the perfusion was switched to 4% PFA. Once the animal was stiff, the system was turned off and the brain was dissected. Brains were then incubated in PFA 4% for 2h-4h at 4ºC after which they were washed in PBS and stored at 4ºC. To preserve the organic tissue, the samples were incubated with Sucrose 20% in PBS before slicing. Slices were cut on a sliding microtome (SM 2000 R) to a thickness of 50µm and collected to a 24-well plate with PBS.

5. mGRASP fluorescent detection and confocal imaging

Two different immunofluorescent approaches were used to test the presence of reconstituted mGRASP signal within the corticostriatal circuit. According to the initial report[80], the mGRASP signal can be seen without the need of post-hoc immunolabelling. However, the signal can be amplified with anti-GFP antibodies[92].

The V12 Lumar fluorescent stereo microscope (Axio Vision 4.8.2/ Hamamatsu Digital CCD Camera C8484) was used to select slices with dTomato-positive neurons for mounting or immunostaining using the Red (Rhodamine) filter. Selected slices were rinsed in 0.1M PB (pH 7.2) to remove crystals of salt that could cause autofluorescence[80]. In a subset of experiments, an incubation step with 1mM glycine was tested to quench free aldehydes in order to reduce background fluorescence. When immunostaining was not performed, the slices were mounted on a glass coverslip (Deckgläser, 24 x 50mm, #1.5 thickness) using a brush. Mowiol mounting medium was applied on top of the dried slices and the glass slide was mounted on top. This method reduces the light diffraction through the sample. Nail polish was then used to seal the coverslips. The slides were left to cure at room temperature (RT) for 1 day and stored at 4ºC.

As an attempt to increase mGRASP signal intensity, an immunohistochemistry protocol was performed based on a previous study[92]. The samples were permeabilized with TBS 0.4% Triton-X100 for 30min at RT, blocked with TBS 0.4% Triton-X100 with 5% normal goat serum (NGS, Sigma Aldrich) for 30min at RT and incubated overnight at 4ºC with the following primary antibodies in TBS 0.4% Triton-X100 with 2% NGS: mouse monoclonal anti-GFP (Sigma cat#G6539) at 1:500, rabbit polyclonal anti-GFP Alexa 488-conjugated (Molecular Probes/Invitrogen cat# A21311) at 1:1000 and rabbit polyclonal anti-GFP (rabbit, Invitrogen cat# A11122) at 1:1000. After 5 washing steps with TBS, the slices were incubated with the following secondary antibodies in TBS 0.4% Triton-X100 with 2% NGS for 2h at RT at a 1:1000 dilution: goat anti-mouse Alexa 488 (Molecular Probes/Invitrogen cat# A11029), chicken anti-rabbit Alexa 488 (Molecular Probes/Invitrogen cat # A21441) and goat anti-rabbit Alexa 488 (Molecular Probes/Invitrogen cat #A11034). In the case of the conjugated antibody, both 2h

RT and overnight 4ºC incubation steps were tested. The mounting procedure was the same as mentioned above.

For the mouse monoclonal anti-GFP antibody, an additional blocking step with 1:10 goat anti-mouse IgG (H&L) (Abcam cat#ab6668) in TBS 0.4% Triton X100 with 2% NGS for 2h was performed before primary antibody incubation[94], in a subset of experiments.

Slice imaging was performed on a Zeiss LSM 710 confocal laser scanning microscope using the following objectives, as indicated in the figure legends: 63x Plan Apochromat oil objective (Zeiss) with 1.4 numerical aperture (NA), 25x Plan Apochromat Multi-immersive objective (Zeiss) with 0.8 NA and 40x Plan Apochromat Multi-immersive objective (Zeiss) with 1.3 NA (Glycerol objective; the refraction index of the glycerol solution was matched to the Mowiol mounting medium). The lasers used were the Diode 405-30 and Argon for the 488nm and 561nm laser line. The excitation and emission wavelengths used are described in Erro! Autorreferência de marcador inválida. for the three fluorophores present: GFP, dTomato and mCerulean. The imaging settings and laser settings were tuned to avoid photobleaching and image saturation. The first mGRASP samples, which did not go through the immunohistochemistry protocol, were set with the following imaging settings: 0.89 pinhole aperture, 700-850 Gain, 60-150 digital offset and 7.5 laser power for the GFP channel; 0.77 pinhole aperture, 700-800 Gain, 50-60 digital offset and 1.0 laser power for the dTomato channel; 1.01 pinhole aperture, 600 Gain, 60-100 digital offset and 4.0 laser power for the mCerulean channel. The immunohistochemistry-treated samples had the following settings: 1.0 pinhole aperture, 700 Gain, 60 digital offset and 2.6 laser power for the GFP channel; 0.87 pinhole aperture, 600 Gain, 30 digital offset and 2.0 laser power for the dTomato channel and 1.13 pinhole aperture, 600 Gain, 60 digital offset and 2.6 laser power for the mCerulean channel.

Table 2– Fluorophores' excitation and emission spectra adapted from: Feng et. al, 2014[80].

Fluorophores	Excitation (nm)	Emission (nm)
mCerulean (presynaptic)	405	441 - 485
mGRASP	488	496 - 554
dTomato (postsynaptic)	561	569 - 639

6. Immunohistochemistry and Confocal imaging of ChI and SPNs

The 300µm coronal brain slices utilized in this analysis were previously submitted to electrophysiology recordings and photostimulation, as detailed previously by Morgenstern el at 2016[95]. Channelrhodopsin-2 (ChR2)-assisted circuit mapping (CRAMP) technique was employed to assess the electrophysiological properties of ChI and SPN-neighbouring neurons after corticostriatal axonal stimulation, in PT- or IT-Cre mice expressing ChR2-YFP. These neurons were filled with 3mg/ml biocytin (Sigma) by the patching pipette and later fixed between 2h to overnight in 4% PFA. After PBS washes, the slices were incubated with primary goat anti-choline acetyltransferase (anti-ChAT) antibody (1:1000 to 1:5000,Chemicon/Millipore cat#AB144P) in PBS, 0.4% Triton-X100 and 2% Normal Horse Serum (NHS, Gibco/Thermo Fisher cat#16050-130) for 1h at room temperature (RT), or 2 days at 4°C. Subsequentially, the slices were successively washed in PBS and incubated with the secondary antibodies in PBS 0.4% Triton X100 with 2% NHS 2h at RT: donkey anti-goat Alexa-405 conjugated antibody (1:200 to 1:1000, Abcam cat# ab175664), rabbit polyclonal anti-GFP Alexa 488 conjugated antibody (1:1000, Molecular Probes cat# A21311) and Streptavidin conjugated to Alexa 594 (1:200, Life Technologies cat#16892). Finally, after successive washes the slices were mounted on the coverslip (Deckgläser, 24 x 50mm, #1.5 thickness) with Mowiol mounting media and nail polish was used to seal the slides. The slides were left to cure at room temperature (RT) for 1 day and preserved at 4°C.

The Zeiss LSM 710 Confocal laser scanning microscope was used for image acquisition. The laser settings were tuned to avoid photobleaching and image saturation. The lasers used were the Diode 405-30, DPSS 561-10 and Argon for the 488nm laser line.

The wavelength parameters used for detecting ChAT, YFP and Streptavidin are described in Table 3.

Table 3– Fluorophores' excitation and emission spectra for the image acquisition of ChI and SPNs.

Fluorophores	Excitation (nm)	Emission (nm)
Alexa 405 (ChAT)	405	414 - 478
GFP Alexa 488 (YFP)	488	496 - 554
Streptavidin Alexa 594	594	569 - 639

The 25x Plan Apochromat Multi-immersive objective (Zeiss) with 0.8 NA was used to image the neuronal arbour in detail for later reconstruction, while the 20x Plan Apochromat (Zeiss) 0.8 NA lens was used to image the soma and take overview tilled images of the slice. The images were acquired at 16bits with 1,024x1,024 frame size, optimal depth interval between 0.83-1µm in z-stacks acquisitions and 10% overlap in the case of tiling. For neuronal reconstructions, tiles of 3x3 images were taken within a 70-90µm z-range, 1.27µsec pixel dwell time, 1x digital zoom, 0.87 pinhole aperture, 700 digital Gain, 30 digital offset and 2-2.5% laser power only with the DPSS 561-10 laser. For the ChAT soma-labelled neurons, the images were z-stack acquisitions with 1x digital zoom. Ten planes were selected from z-stacks covering between 10-20µm z-range (to include only the somas), using 1,27µsec pixel dwell time. The DPSS 561-10 was set to the same settings as those used to take images for neuronal reconstructions, Diode 405-30 was set to 1.17 pinhole aperture, 700-750 digital Gain, -1000 to -2000 digital offset and 4-10% laser power. The Argon laser was set to 1 pinhole aperture, 750 digital Gain, 60 digital offset and 2-2.6% laser power.

7. Neuronal reconstruction and Sholl Profile analysis

After stitching the acquired images of individual ChIs or ChI+SPN pairs on FIJI/ImageJ[96], the neurons were reconstructed using the neuTube software[80,81,92] and saved as a SWC file. The tracing was semi-automatized and manually proofread, both at 2D and 3D. To confirm the reconstructed neuronal tracings in a different software, the Simple Neurite Tracer (SNT) plugin on FIJI/ImageJ[97] was used. This plugin also allowed the acquisition of a skeletonized image of the tracings at a real scale, which were used to overlap with the Maximum Intensity Projection (MIP) images and confirm the scaling. The Sholl Analysis plugin on FIJI/ImageJ[98] was used to acquire Sholl profiles of each reconstruction. The radius step size was automatized. However, the data was sorted later for consistency and set at 10µm. The data was potted with GraphPad/Prism 6 (La Jolla, CA, USA) software, where the mean and s.e.m were also calculated.

Results

We designed a series of mGRASP experiments with the aim of characterizing the distribution, number and location of corticostriatal synapses onto SPNs. We reasoned that by expressing pre-mGRASP in cortical neurons (presynaptic), together with post-mGRASP in SPNs (postsynaptic), synaptic contacts would become detectable. To examine the connections between specific neuronal populations, the Cre/LoxP system was employed together with adeno-associated viral (AAV) injections and transgenic Cre-mouse lines. For achieving selective labelling in cortical presynaptic neurons, we injected AAV-Cre-dependent 'switch off' pre-mGRASP in the motor cortex (MC) in PT-Cre or IT-Cre mice. On the other hand, for postsynaptic D1-SPN selective expression, we injected AAV-Cre-dependent 'switch on' post-mGRASP in the dorsolateral striatum (DLS), using D1-Cre mice.

We first decided to troubleshoot the AAV delivery to the MC, to ensure a robust fluorescent labelling in the axonal projections from presynaptic cells, and the DLS viral mix conditions to obtain sparse labelling of postsynaptic neurons. For this, we tested different AAVs expressing fluorescent proteins.

1. Optimization of AAV injection conditions

1.1. Cortical AAV injections

Our first optimization step was to maximize the density of labelled cortical axons with pre-mGRASP in the ipsilateral dorsolateral striatum. We injected AAV9-ChR2-mCherry at an Anterior-Posterior (AP) distance of +0.8mm from bregma following the Allen Mouse Brain Connectivity Atlas (with mediolateral (ML) +1.6mm and dorsoventral (DV) -0.75mm from bregma and the surface of the skull, respectively). After 3 weeks of viral expression, brain slices from 2 wildtype mice were analysed by confocal imaging. Consistent with what was expected, the viral injections at AP=+0.8mm revealed an overall broad axonal label in the DLS (Figure 11)

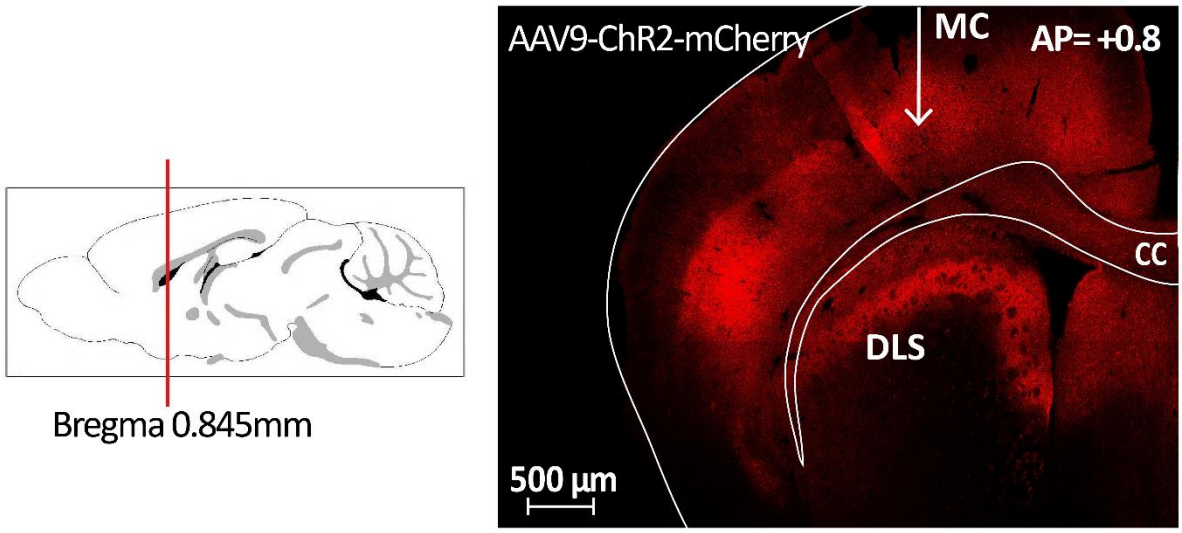

Figure 11 – Anterior-posterior location of cortical AAV injections for optimal axonal projection labelling in the DLS. Left panel, Diagram of a sagittal brain slice showing the anterior-posterior (AP) location where AAV9-ChR2-mCherry was injected to ensure dense axonal labelling in dorsolateral striatum (DLS). Right panel, Representative single plane image (10x objective) of a brain slice showing the axonal density in the ipsilateral cortex and DLS when the AAV injection was performed at AP location +0.8 mm according to bregma (n=2 wildtype mice). The mediolateral (ML) and dorsoventral (DV) coordinates were +1.6mm and -0.75mm from bregma and the surface of the skull, respectively. *MC – motor cortex, CC-corpus callosum*.

1.2. Striatal AAV injections

We next tested a combination of two AAVs to achieve sparse labelling of striatal neurons. The main goal was to express an "inducer" AAV expressing Cre at a low titter, limiting the number of cells infected. A second Cre-dependent AAV, used at high titter, would then express a fluorescent protein through Cre-recombinase induction. Thus, only a small subset of cells would be labelled, while maintaining a high level of fluorophore expression per cell.

First, we injected AAV-Cre together with a well-established AAV expressing GFP in a Cre-dependent manner, rAAV1-FLEX-GFP, at a 1:4 mix in the DLS. After 3 weeks of expression we imaged 10 corticostriatal slices from 4 animals and checked the density of labelled neurons. We tested 6 different dilutions, 1:10, 1:100, 1:300, 1:700, 1:1000 and 1:10000, and four of them are represented in Figure 12. From the results gathered, AAV-Cre diluted at 1:700 up to 1:1000 ($6.383x10^9$ gc/ml and $4.648x10^9$ gc/ml, respectively) showed an adequate number of sparsely labelled neurons in the slices analysed (Figure 12).

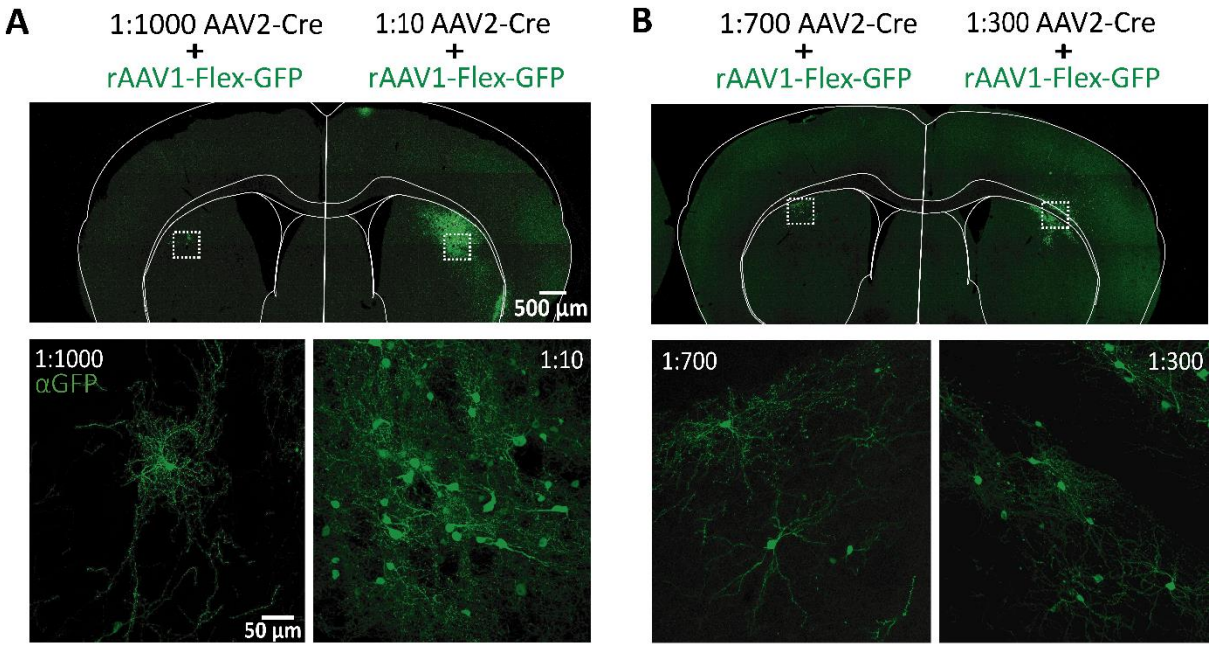

Figure 12 – Troubleshooting AAV-Cre dilutions to achieve sparse fluorescent labelling on striatal neurons. AAV-Cre and a second AAV expressing GFP in a Cre-dependent manner (rAAV1-Flex-GFP) were injected at 1:4 dilution in the DLS (AP=+0.8mm, ML=±2.3mm, DV=-2mm). Top panels, Representative single plane brain slice overviews (10x objective) of the viral infection spread at the different dilutions of AAV-Cre: 1:1000, 1:10 in panel A (n=2 wildtype mice), and 1:700, 1:300 in panel B (n=2 wildtype mice). Bottom panels, Higher magnification z-stack images (20x objective) of the DLS regions represented as squares in the corresponding top panels depicting the density of GFP-labeled striatal cells at the different AAV-Cre dilutions.

Taking into consideration the sparseness of the signal in the previous approach, we then extended our AAV-Cre dilution optimization to the post-mGRASP component. The AAV used for the post-mGRASP, termed here CreONPost (AAV-ON-post-mGRASP-2A-dTomato), expresses the split GFP1-10 and dimeric Tomato (dTomato) in a Cre-dependent manner, which allows the visualization of the postsynaptic cells. While the 1:700 and 1:1000 dilutions were optimal for GFP sparse labelling using rAAV1-FLEX-GFP, it resulted in a dTomato expression that was too sparse (data not shown and Figure16C). Therefore, we tested AAV-Cre diluted 1:100 and 1:500 and both dilutions induced an adequate density of striatal cells labelled with dTomato (Figure 13, n=2 mice). We decided to use both AAV-Cre dilutions in subsequent experiments.

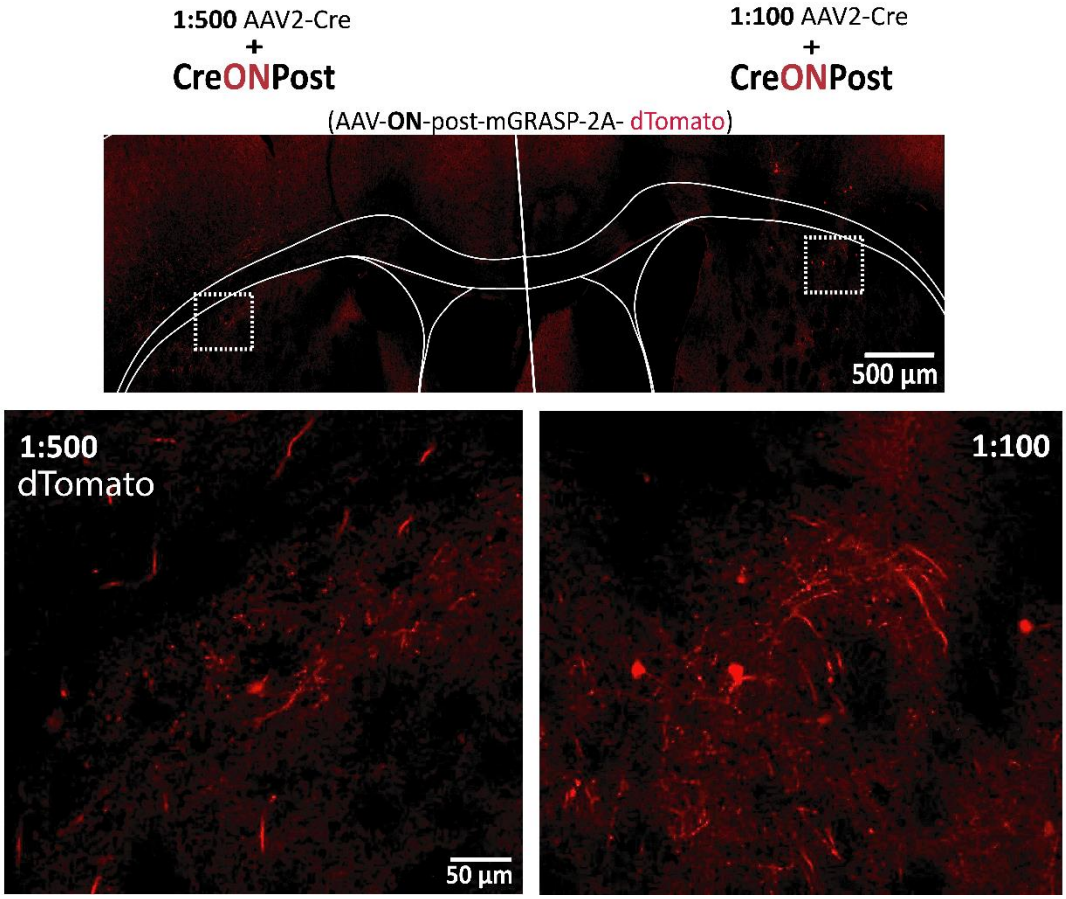

Figure 13- Troubleshooting AAV-Cre dilutions to achieve sparse expression of post-mGRASP in the DLS. AAV-Cre and a second AAV expressing the post-mGRASP construct in a Cre-dependent manner (AAV-ON-post-mGRASP-2A-dTomato, designated CreONPost for simplicity) were injected at 1:4 dilution in the DLS (AP=+0.8mm, ML=±2.3mm, DV=-2mm). Top panels, Representative single plane brain slice overview (20x objective) of the viral infection spread of AAV-ON-post-mGRASP-2A-dTomato at the 1:100 and 1:500 dilutions (n=2 mice). Bottom panels, Amplified digital crops of the DLS regions represented as squares in the corresponding top panels, showing the density of dTomato-labelled neurons (n=2 PT-Cre mice).

2. Testing mGRASP between motor cortex and DLS neurons

After the optimization steps, two main approaches were tested in accordance to the protocol designed previously for mGRASP[80,81]. To detect the intrinsic signal of mGRASP reconstitution, mice were injected with pre-mGRASP in the motor cortex and post-mGRASP in the DLS.

2.1. First approach with D1-Cre mice

As a first approach, we addressed IT contralateral connections with D1-SPNs, using D1-Cre transgenic animals. Mice were stereotaxically injected with Cre-independent pre-mGRASP (AAV-pre-mGRASP-mCerulean-2A-NLS-mCherry) in the MC of the right hemisphere (n=2 mice) (Figure 14A). Besides the split GFP11, this AAV also expresses monomeric Cerulean (mCerulean) in the cytosol, which labels corticostriatal axons, and monomeric Cherry

(mCherry) with a nuclear localization sequence, which labels the nuclei of infected cells in the MC. The latter evidences the injection site and allows better slice selection for imaging (detailed in the method section).

The second injection was in the contralateral dorsolateral striatum (left hemisphere) of the same D1-Cre mice, with the CreONPost AAV (AAV-ON-post-mGRASP-2A-dTomato) (n=2 mice). Given that PT axons do not cross the midline, this strategy provides specificity to study IT axons. We found the dTomato signal to be visible along the dendrites of infected postsynaptic cells (Figure 14C). The results suggest a correct expression of both pre and post-mGRASP components by their fluorescent label in the pre and postsynaptic infected neurons. However, some line-like non-specific signals were also evident (Figure 14B). This phenomena was already documented previously[81] in relation to CD4-based GRASP systems, and, therefore, it was expected.

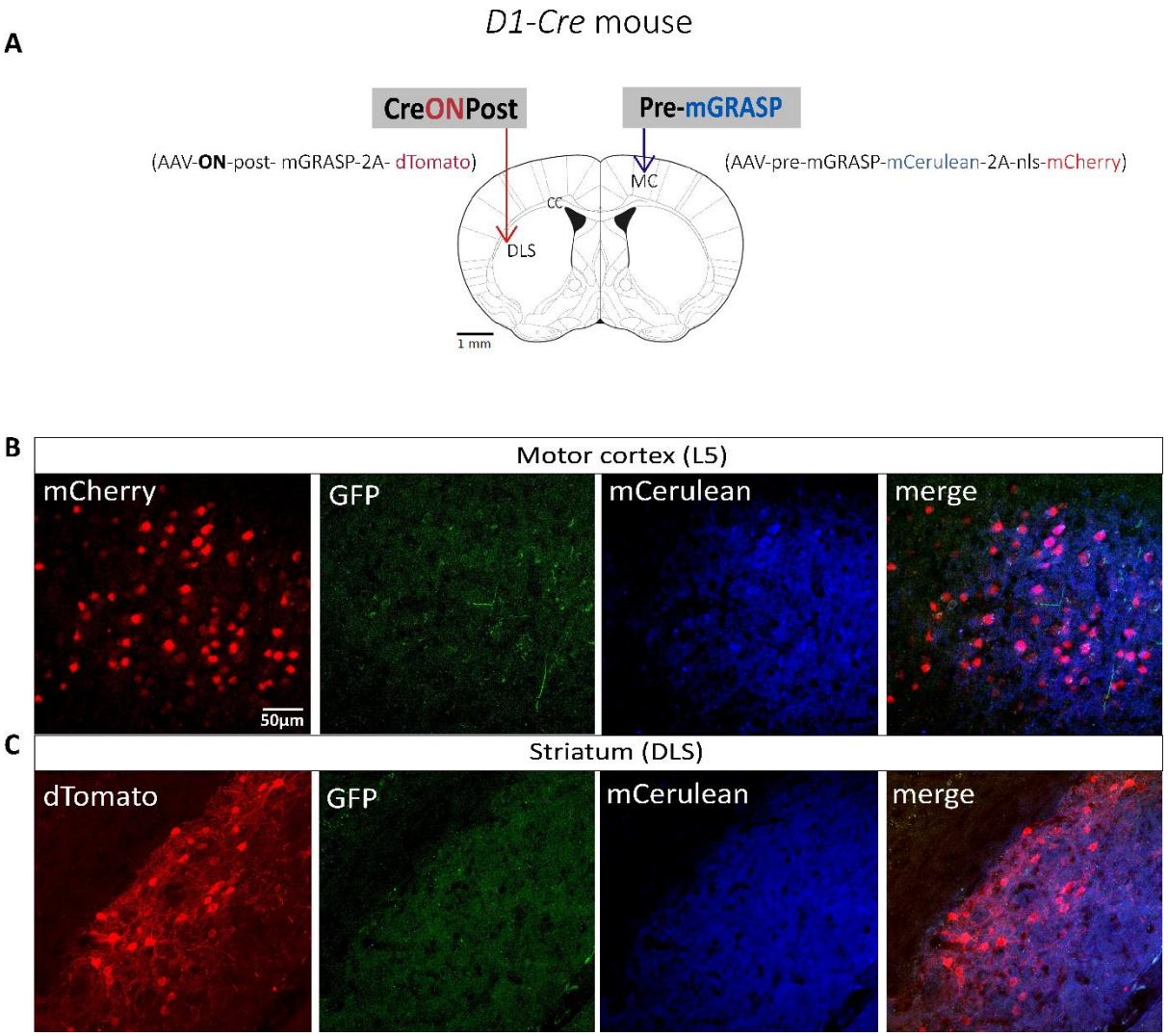

Figure 14 - Testing mGRASP between IT cortical neurons expressing pre-mGRASP and D1-SPNs expressing post-mGRASP, in D1-Cre mice. A, Schematic representation of the viral delivery strategy. D1-Cre mice were injected with a Cre-independent pre-mGRASP construct (AAV-pre-mGRASP-mCerulean-2A-NLS-mCherry or

Pre-mGRASP for simplicity) in the right motor cortex (MC; AP=+0.8mm, ML=+1.6mm, DV=-0.75mm), and a Cre-dependent post-mGRASP construct (AAV-ON-post-mGRASP-2A-dTomato or CreONPost) in the left DLS (AP=+0.8mm, ML=-2.3mm, DV=-2mm). In addition to the pre and postsynaptic split-GFP isoforms, the Pre-mGRASP construct expresses both cytosolic mCerulean and mCherry with a nuclear localization sequence, while CreONPost expresses cytosolic dTomato. The left DLS receives mCerulean-positive IT cortical projections from the right hemisphere. B, Representative maximal intensity projections (MIPs) of image z-stacks (25x objective) of mCherry, GFP and mCerulean signals in the right MC (ipsilateral to Pre-mGRASP injection; n=2 mice). C, Representative MIPs of image z-stacks (25x objective) of dTomato, GFP and mCerulean signals in the left DLS, contralateral to Pre-mGRASP injection and ipsilateral to CreONPost injection (n=2 mice). *CC- corpus callosum*

We next analysed higher magnification images of putative mGRASP-specific and non-specific signals. Some resemble the mGRASP signals reported previously in hippocampal slices (Figure 15A,B,D,E, white arrows)[92]. The mGRASP signal is reconstituted on the synaptic cleft, in between the labelled blue and red neuronal structures[81,86,99]. The synaptic cleft is less than 100 nm wide and the signals were expected to be close to a dendrite or shaft, not completely overlapping with the red signal, as it is reconstituted extracellularly[86]. In our images, only in a few cases the size and the distance to a neighbouring dendrite seem to match what was expected (Figure 15B,E, white arrows). However, in most cases the signals detected in the green channel did not resemble synapses (Figure 15A,C,D,F, yellow arrows). Not only the signals overlapped in both red and green channels, but also, the size and distribution of the signals away from the labelled dendrites suggests that these do not represent reconstituted GFP from mGRASP. In addition, there were also green non-specific signals detected in the MC (as represented in Figure 14B), which further shows a low signal-to-noise ratio.

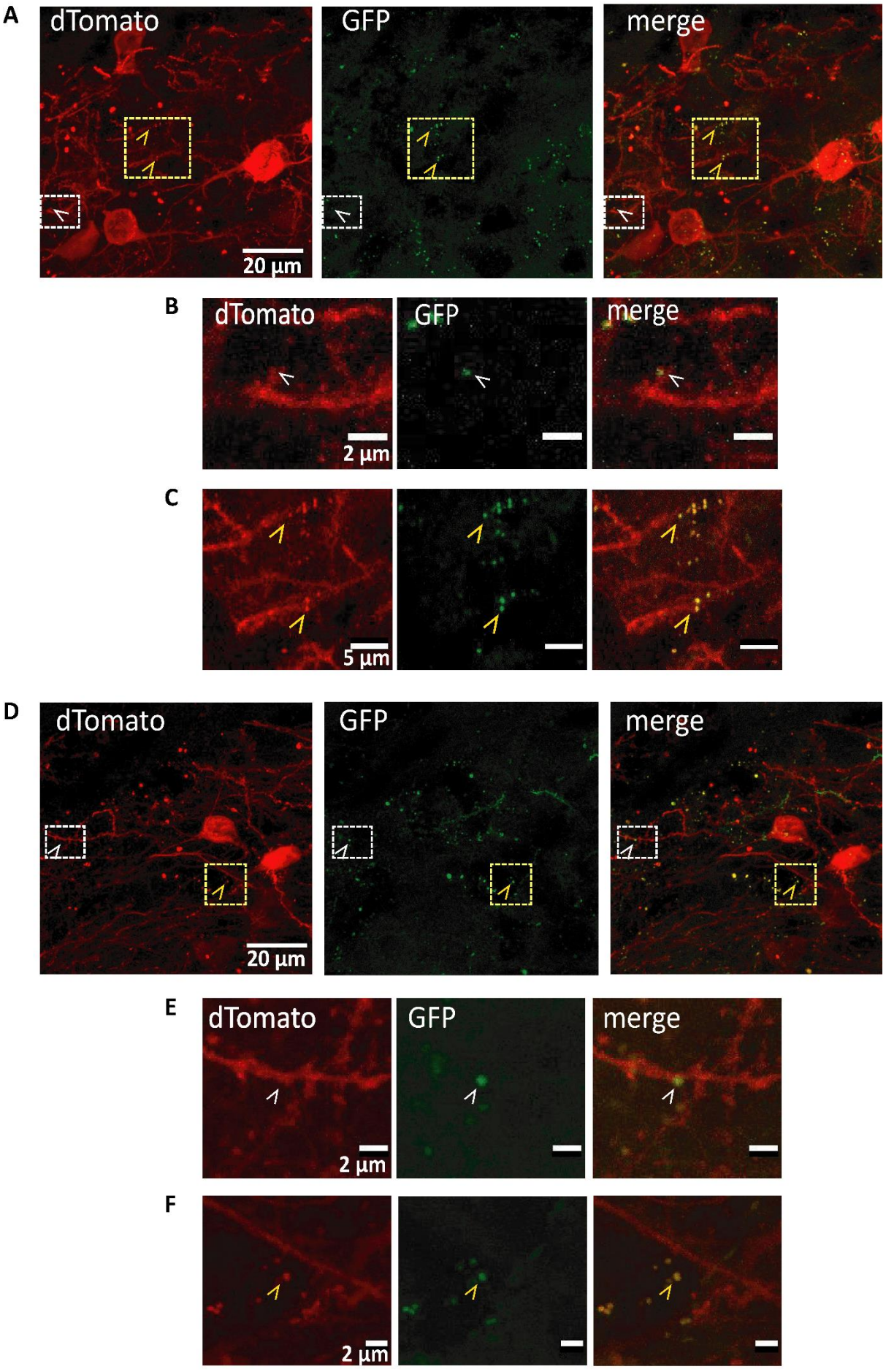
A
dTomato
GFP
merge
20 µm
B
dTomato
GFP
merge
2 µm
C
5 µm
D
dTomato
GFP
merge
20 µm
E
dTomato
GFP
merge
2 µm
F
2 µm

Figure 15 - Higher magnification images from putative mGRASP specific and non-specific signals obtained with pre-mGRASP-expressing IT cortical neurons and post-mGRASP-expressing D1-SPNs, in D1-Cre mice. A similar viral delivery strategy to that described in the legend of Figure 4A was used to express Pre-mGRASP in cortical neurons and CreONPost in D1-SPNs of the DLS. A,D, Two examples of representative MIPs of image z-stacks (63x objective) showing dTomato and GFP signals in the DLS (n=2 mice). B,E, Digitally cropped images of the DLS regions depicted as white squares in the corresponding A and D panels. Putative mGRASP signals localized near dTomato-labeled dendritic spines or shafts are indicated by white arrows (close apposition of both green and red signals was confirmed on single z planes). C,F, Digitally cropped images of the regions depicted as yellow squares in A and B. Yellow arrows indicate putative non-specific signals that are visible in both red and green channels.

2.2. Second approach with PT-Cre mice

Our next approach was to address cortical connections from IT neurons onto SPNs in the DLS of the same hemisphere, in PT-Cre mice. Ipsilateral IT projections are denser than the contralateral ones[9]. Thus, we wondered whether increasing the density of labelled axons would enhance the probability of visualizing mGRASP signals. On the other hand, the D1 selectivity for the post-mGRASP component would be compromised. We developed a combination of AAV-Cre and CreONPost (AAV-ON-post-mGRASP-2A-dTomato) that allowed sparse labelling on striatal neurons, which would support the analysis of single SPNs sampling specific cortical inputs. Mice were injected with pre-mGRASP Cre-dependent 'switch off', here termed CreOFFPre (AAV-pre-mGRASP-mCerulean), in the MC. Next, mice were injected ipsilaterally with a 1:1000 AAV-Cre and CreONPost mix, on the DLS (Figure 16A) (n=2 mice). We found that the dTomato signal was very sparse (Figure 16C), prompting the AAV-Cre dilution test depicted in Figure 13 and the selection of higher concentrations of AAV-Cre in subsequent experiments. Nevertheless, green puncta-like signals persisted (Figure 16B,C), suggesting that most of those signals were non-specific. Consistent with the previous results, the signal-to-noise ratio was very low.

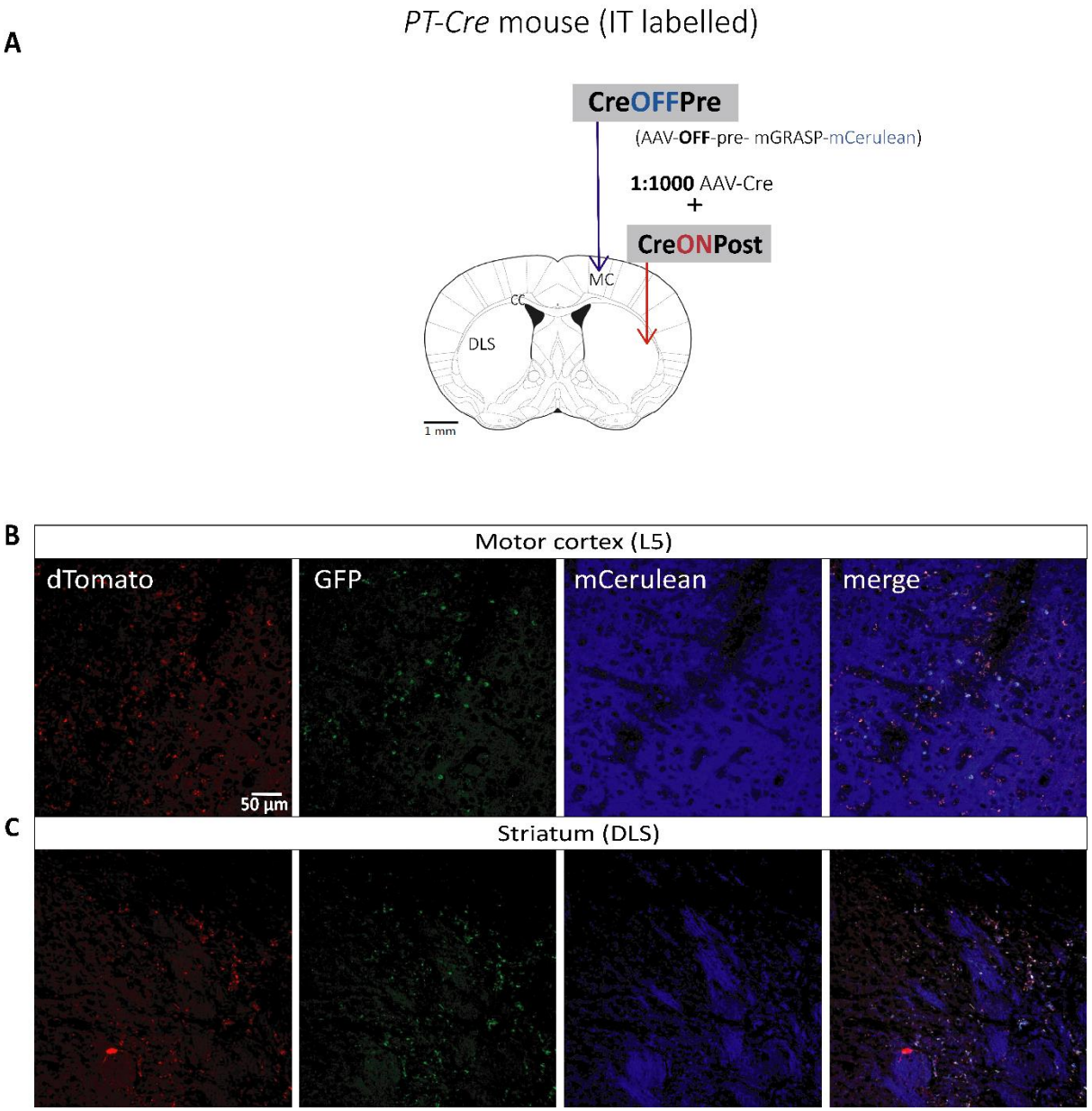

Figure 16 - Testing mGRASP between pre-mGRASP-expressing IT cortical neurons and post-mGRASP-expressing striatal neurons, in PT-Cre mice. A, Schematic representation of the viral injection strategy. PT-Cre mice were injected with a Cre-dependent CreOFFPre construct (AAV-OFF-pre-mGRASP-mCerulean) in the right motor cortex (MC; AP=+0.8mm, ML=+1.6mm,DV=-0.75mm), and a combination of AAV-Cre at 1:1000 and CreONPost (AAV-ON-post-mGRASP-2A-dTomato) at a 1:4 mix in the ipsilateral DLS (AP=+0.8mm, ML=+2.3mm, DV=-2mm), to achieve SPN sparse labeling. The CreOFFPre construct expresses pre-mGRASP and mCerulean in cells that do not express Cre at injected cortical layer 5 of PT-Cre mice, i.e., IT neurons. B,C, Representative single plane images (20x objective) of dTomato, GFP and mCerulean signals in the MC (B) and DLS (C) (n=2 mice). *CC- corpus callosum.*

To better understand the limitations of the mGRASP method, we designed a control experiment where PT-Cre mice were injected only with 1:100 AAV-Cre + CreONPost in the right dorsolateral striatum (Figure 17A). In the absence of the pre-mGRASP component, the

GFP reconstruction would not occur and any specific signal would be absent. In this scenario, non-specific signals would become evident. The results showed that most of the green signal in the DLS was still present, demonstrating that it is indeed non-specific (Figure 17B,C). Moreover, overlapping puncta-like signals in both green and red channels suggest the presence of fluorescent particles in the tissue. We reasoned that the presence of this non-specific signal could be confounding for the detection of the mGRASP signal in previous experiments.

In an attempt to improve the mGRASP specific signal, a glycine incubation step was added to the protocol, as it was previously suggested to quench free aldehydes from the slices and increase the signal-to-noise ratio[81]. The brain slices that were used in this procedure were from the same mice as in Figure 17, and, therefore, the improvement could be assessed within similar samples. Nevertheless, the overlapping puncta-like signals remained evident after glycine incubation (Figure 18B,C). We argued that since the non-specific signal could not be reduced, the specific signals would have to be amplified to allow mGRASP detection.

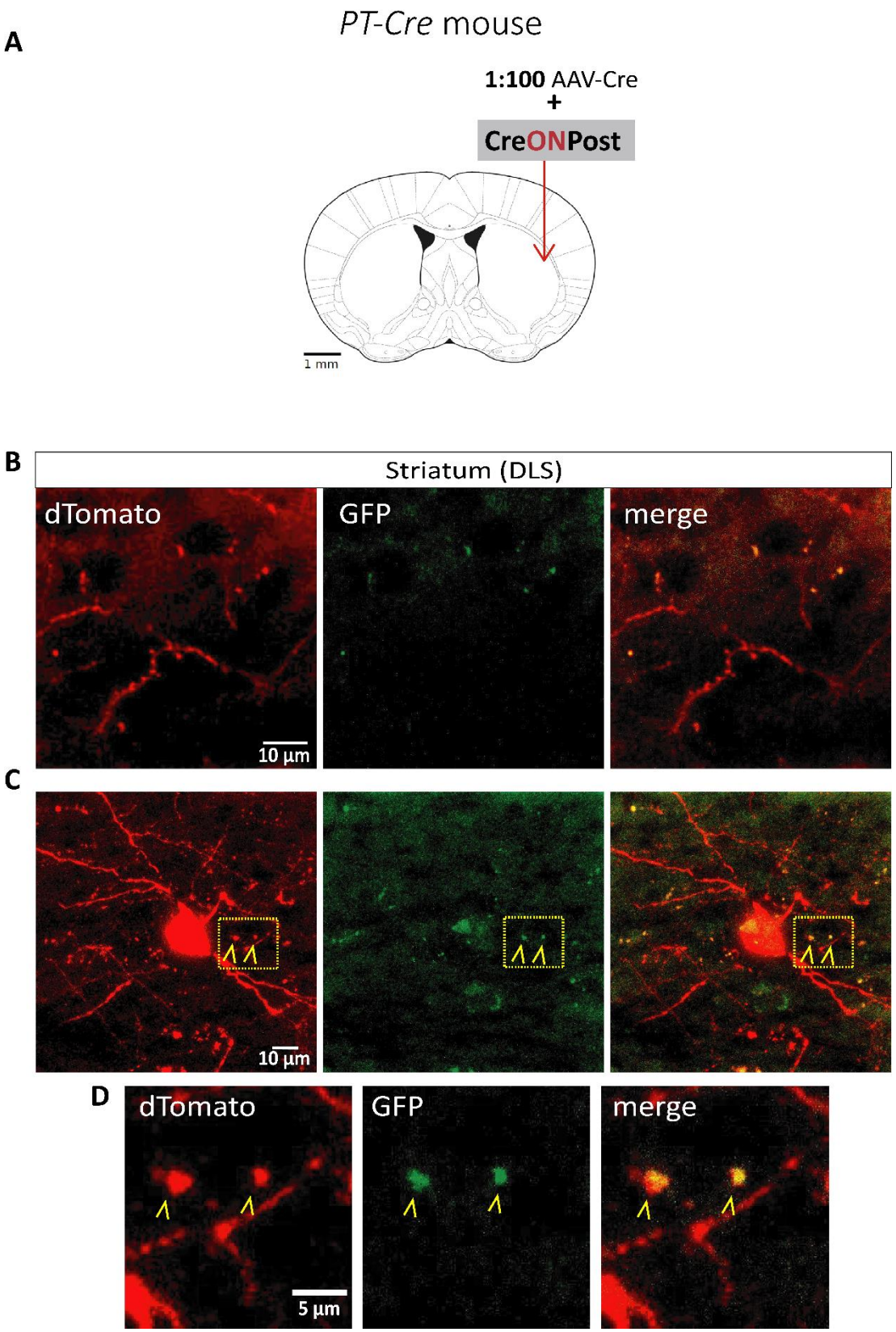

Figure 17 - Control experiment in PT-Cre mice injected only with the post-mGRASP construct in the DLS. A, Schematic representation of the viral injection strategy. PT-Cre mice were injected with a combination of AAV-Cre at 1:100 and CreONPost (AAV-ON-post-mGRASP-2A-dTomato) at a 1:4 mix in the DLS. B,C, Representative MIPs of image z-stacks (40x objective) showing dTomato and GFP signals in the DLS (n=1 mouse). D, Digitally

cropped images of the region depicted as a yellow square in C. Yellow arrows indicate putative non-specific signals that overlap in both red and green channels. *MC-motor cortex, CC- corpus callosum.*

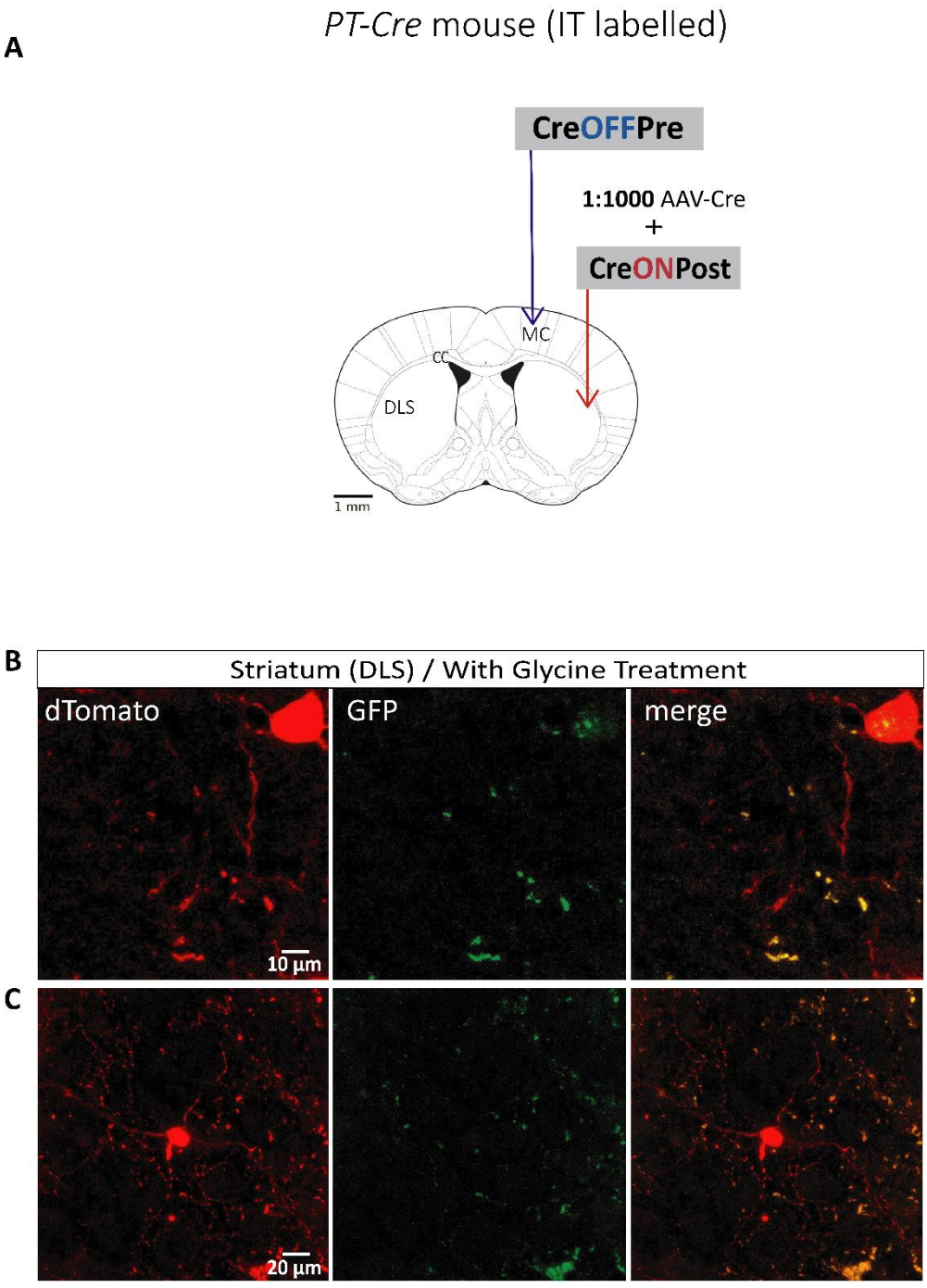

Figure 18 - Testing glycine treatment on mGRASP experiment between pre-mGRASP-expressing IT neurons and post-mGRASP-expressing striatal neurons, in PT-Cre mice. A- Schematic representation of the viral injection strategy (detailed in the legend of figure 6A). B,C – Representative MIPs of image z-stacks (40x objective) of dTomato and GFP signals in the DLS (n=1 mouse). *CreOFFPre- AAV-OFF-pre-mGRASP-mCerulean, CreONPost- AAV-ON-post-mGRASP-2A-dTomato, MC-motor cortex, CC- corpus callosum*

2.3- Amplification of the GFP signal with immunolabeling

Thus far, our data could not support a robust and conclusive split-GFP reconstitution over the synaptic clefts between pre- and postsynaptic labelled neurons. Therefore, we next sought to assess if the reconstituted GFP signal could be amplified through immunofluorescent staining with anti-GFP antibodies (Table 4).

Table 4 -Antibodies tested for specificity towards reconstituted GFP.

Antibody reference	Antibody description	Abbreviation	Dilution used
Invitrogen cat#A11122	Rabbit polyclonal anti-GFP	αGFP-RpAb	1:1000
Molecular probes/Invitrogen cat#A21311	Rabbit polyclonal anti-GFP conjugated with Alexa 488	αGFP-RpAb-A488	1:1000
Sigma cat#G6539	Mouse monoclonal anti-GFP	αGFP-MmAb	1:500

2.3.1 Immunolabelling against GFP with a rabbit polyclonal antibody

In GRASP implemented methods for studying *Drosophila*'s neuronal circuits, some antibodies detected the GFP reconstituted form with high specificity, showing little to no signal upon expression of their split GFP counterparts[100]. We reasoned that if the polyclonal anti-GFP antibody had robust affinity for the mGRASP, it would increase the likelihood of detecting the specific puncta signal. Nevertheless, as a polyclonal antibody, we regarded the possibility of recognizing the pre- and/or post-mGRASP constructs[92].

PT-Cre mice were injected with CreOFFPre (AAV-pre-mGRASP-mCerulean) in the MC and a viral mix of 1:100 AAV-Cre + CreONPost (AAV-ON-post-mGRASP-2A-dTomato) in the DLS (Figure 19A). We found that this antibody was not selective for the reconstituted form of GFP, as it elicited green signals in the MC where the reconstitution is not expected, probably due to binding to pre-mGRASP (Figure 19B,C). In addition, we observed that the antibody recognized the post-mGRASP component, as it can be observed by the overlap of green signals on dTomato positive neurons (Figure 19D). Moreover, the pattern of green immunofluorescent label in the DLS and along the *corpus callosum* suggests split GFP expression along the axonal projections of pre-mGRASP infected neurons (Figure 19B,C). Despite this antibody not being useful for mGRASP signal amplification, it confirmed the correct expression of the pre- and post-mGRASP components.

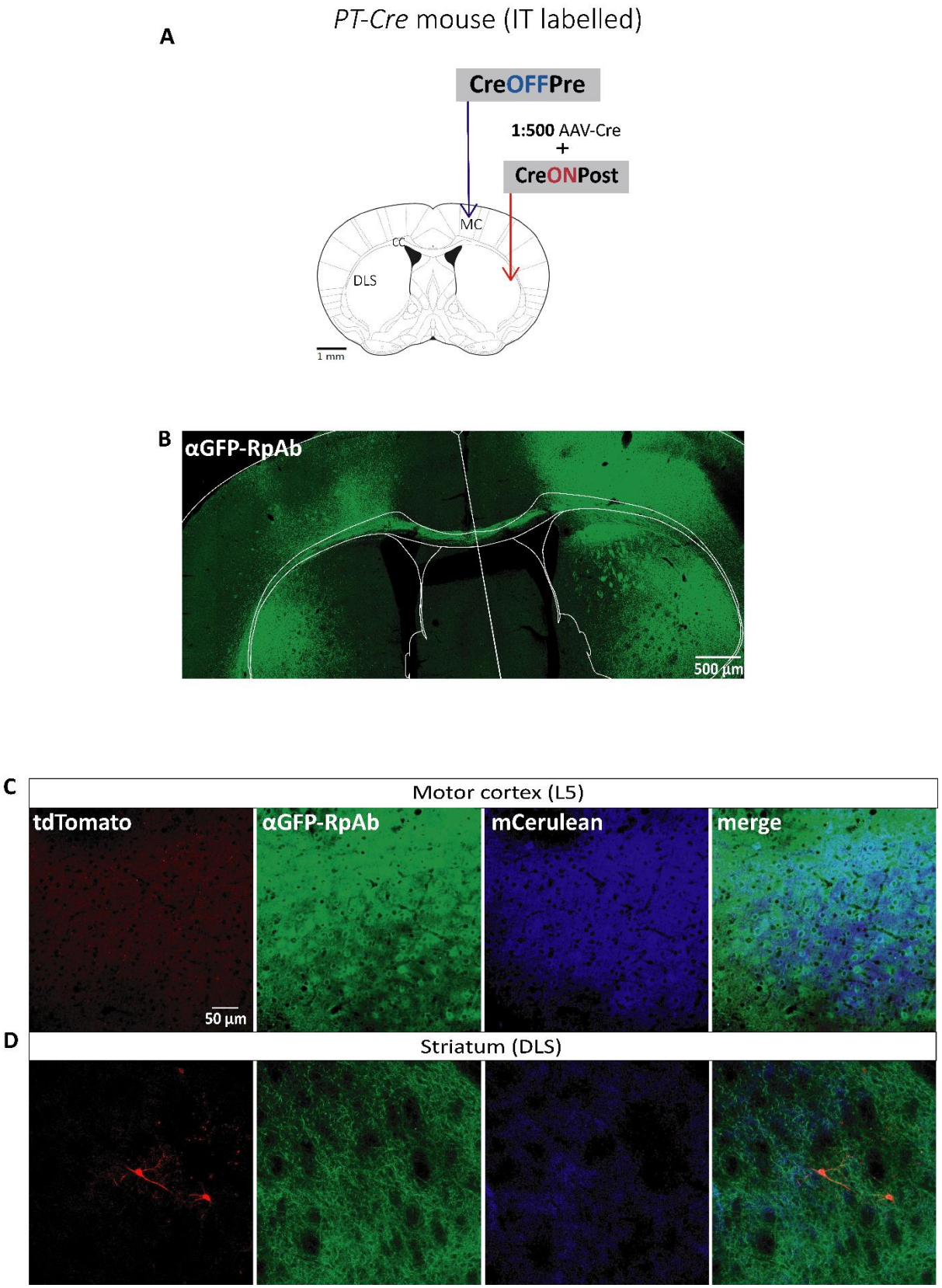

Figure 19 - Testing mGRASP signal amplification using a rabbit polyclonal anti-GFP antibody in a PT-Cre mouse, expressing pre-mGRASP in IT neurons and post-mGRASP in striatal neurons. A, Schematic representation of the viral injection strategy (as detailed in the legend of figure 6A, apart from the AAV-Cre dilution that was 1:500). B, Representative single plane image (20x objective) of a brain slice immunolabelled

against GFP using a rabbit polyclonal anti-GFP antibody (GFP-RpAb) at 1:1000. C,D, Representative single plane images (20x objective) of dTomato, anti-GFP and mCerulean signals in the motor cortex (MC) in C and DLS in D (n=1 mice). *CreOFFPre- AAV-OFF-pre-mGRASP-mCerulean, CreONPost- AAV-ON-post-mGRASP-2A-dTomato, CC- corpus callosum.*

We next designed a control experiment, in which only the post-mGRASP isoform was expressed in the DLS of PT-*Cre* mice, without expressing the pre-mGRASP component in the MC (Figure 20A). As previously noted, the antibody recognized the post-mGRASP construct in the DLS (Figure 20B,C), further illustrating the lack of selectivity towards the reconstituted GFP and the correct expression of the post-mGRASP component.

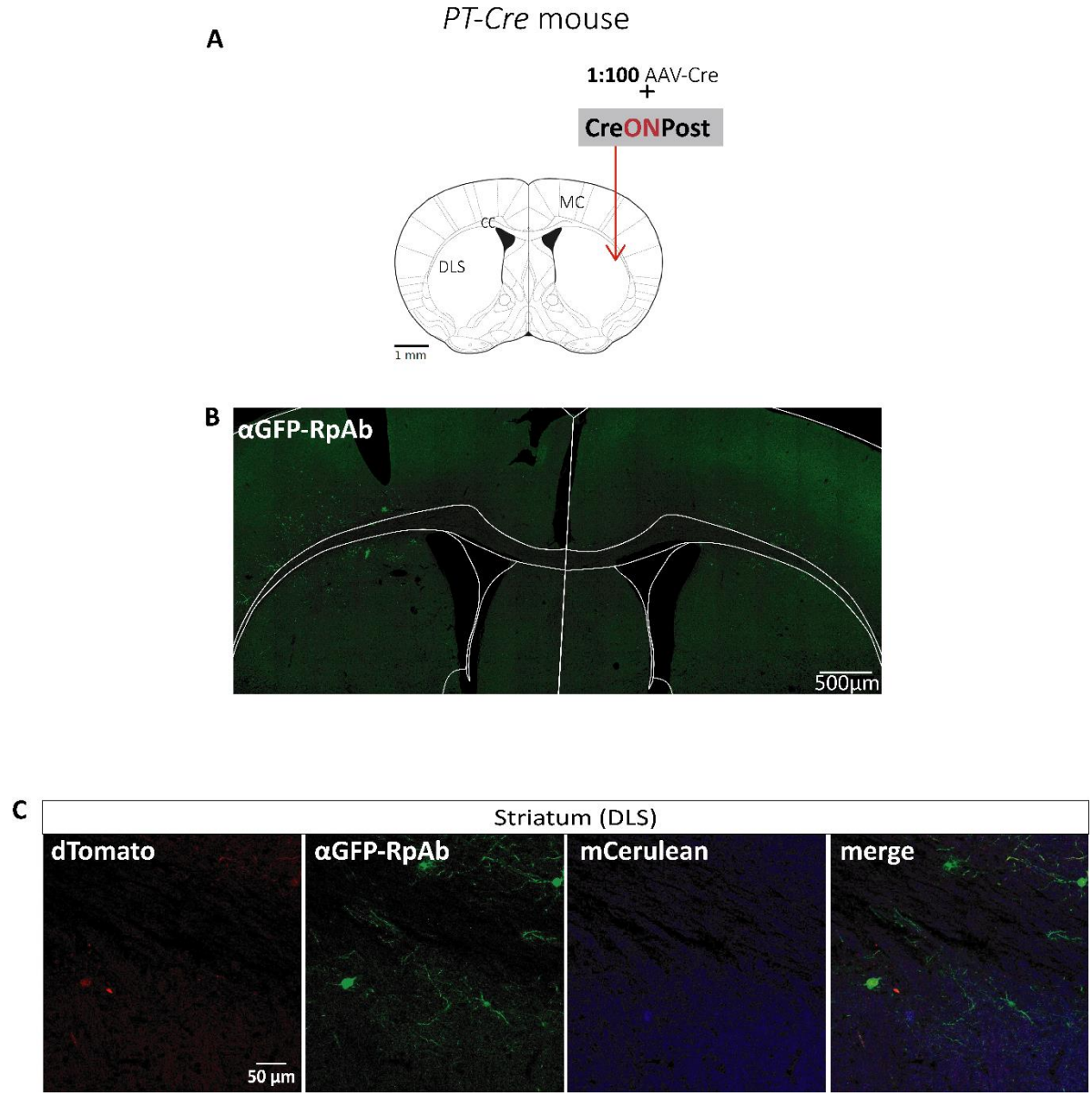

Figure 20 - Testing recognition of post-mGRASP by the rabbit polyclonal anti-GFP antibody using a PT-Cre mouse injected with only the post-mGRASP construct in the DLS. A, Schematic representation of the viral strategy (as detailed in the legend of figure 7A). B, Representative single plane image (20x objective) of a brain

slice immunolabelled against GFP using a rabbit polyclonal anti-GFP antibody (GFP-RpAb) at 1:1000. C, Representative images of dTomato, GFP and mCerulean signals in the DLS (n=1 mice). *MC – motor cortex, CC- corpus callosum.*

2.3.2- Immunolabelling against GFP with a rabbit polyclonal antibody conjugated with Alexa 488

Our next assay was to test a different antibody, in an effort to achieve mGRASP reconstituted specificity. PT-Cre mice were injected with CreOFFPre (AAV-pre-mGRASP-mCerulean) in the MC and 1:500 AAV-Cre + CreONPost (AAV-ON-post-mGRASP-2A-dTomato) in the DLS (Figure 21A). We used a different rabbit polyclonal anti-GFP conjugated with Alexa 488, incubating the brain slices for 2h or overnight in an effort to reduce unspecific binding. Though, neither the 2h (data not shown) nor the overnight (Figure 21B-D) incubation conditions produced selective binding of the antibody to the reconstituted GFP. The antibody recognized the pre-mGRASP component, as the green signal co-localized with the mCerulean signal in the MC (Figure 21C). Moreover, in the DLS and the *corpus callosum*, the green label resembles axonal projections from presynaptic cells (Figure 21B,D).

We also observed that the rabbit polyclonal anti-GFP conjugated with Alexa 488 antibody recognizes the post-mGRASP positive cells in the DLS of PT-Cre animals expressing only CreONPost (Figure 22). Though this antibody was also not selective for the reconstituted form of GFP, these results confirm that the pre- and post-mGRASP components were robustly expressed in the pre and postsynaptic neurons, respectively (Figure 21, 22).

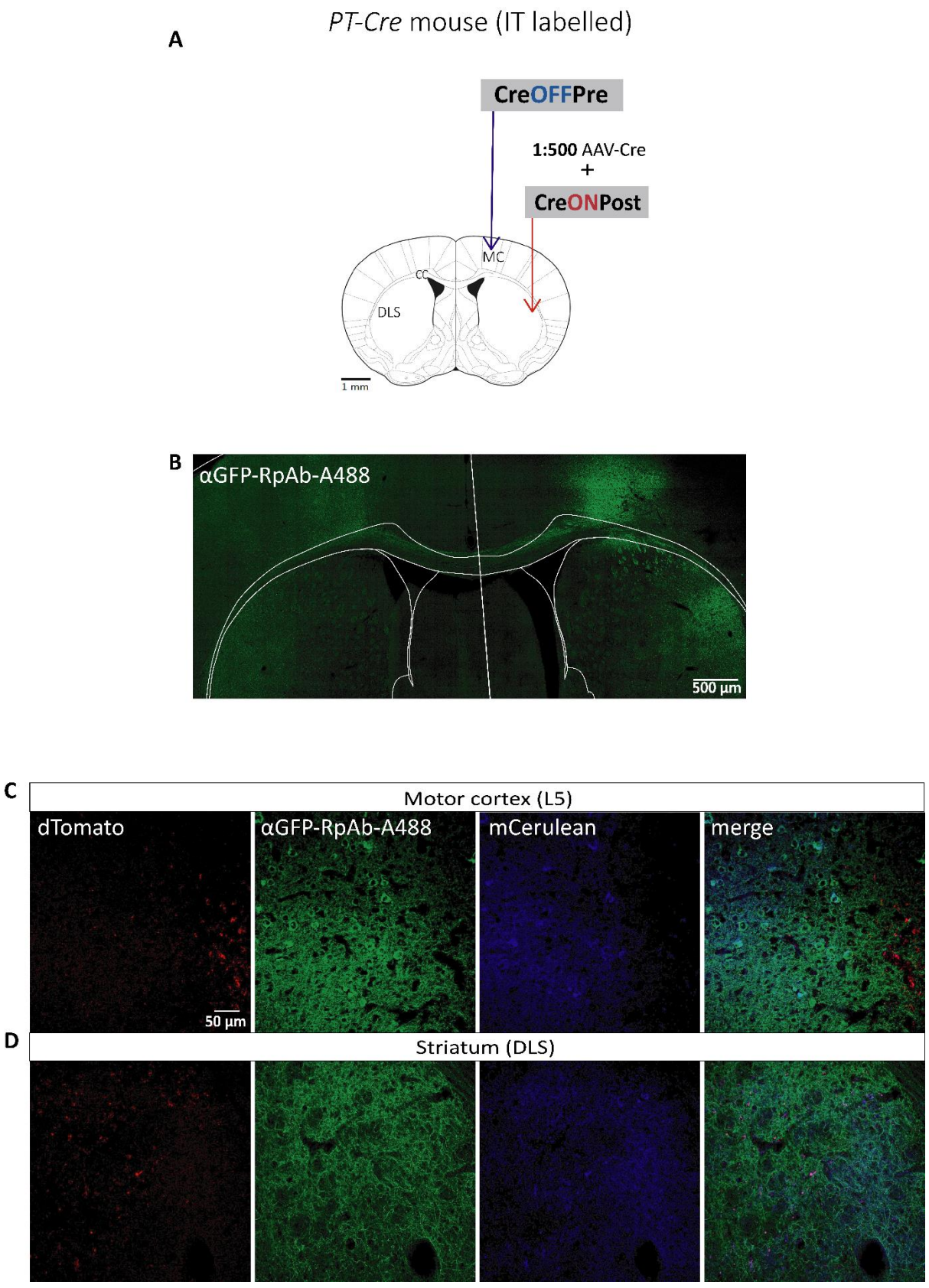

Figure 21 - Testing mGRASP signal amplification using a rabbit polyclonal anti-GFP antibody conjugated with Alexa 488 in PT-Cre mice, expressing pre-mGRASP in IT neurons and post-mGRASP in striatal neurons. A, Schematic representation of the viral strategy (as detailed in the legend of figure 6A, apart from the AAV-Cre

dilution that was 1:500). B, Representative single plane image (20x objective) of a brain slice immunolabelled against GFP using a rabbit polyclonal anti-GFP antibody conjugated with Alexa 488 (GFP-RpAb-A488) at 1:1000. C,D, Representative images of dTomato, anti-GFP and mCerulean signals in the motor cortex (MC) in C and DLS in D (n=1 mice). *CreOFFPre- AAV-OFF-pre-mGRASP-mCerulean, CreONPost- AAV-ON-post-mGRASP-2A-dTomato, CC- corpus callosum.*

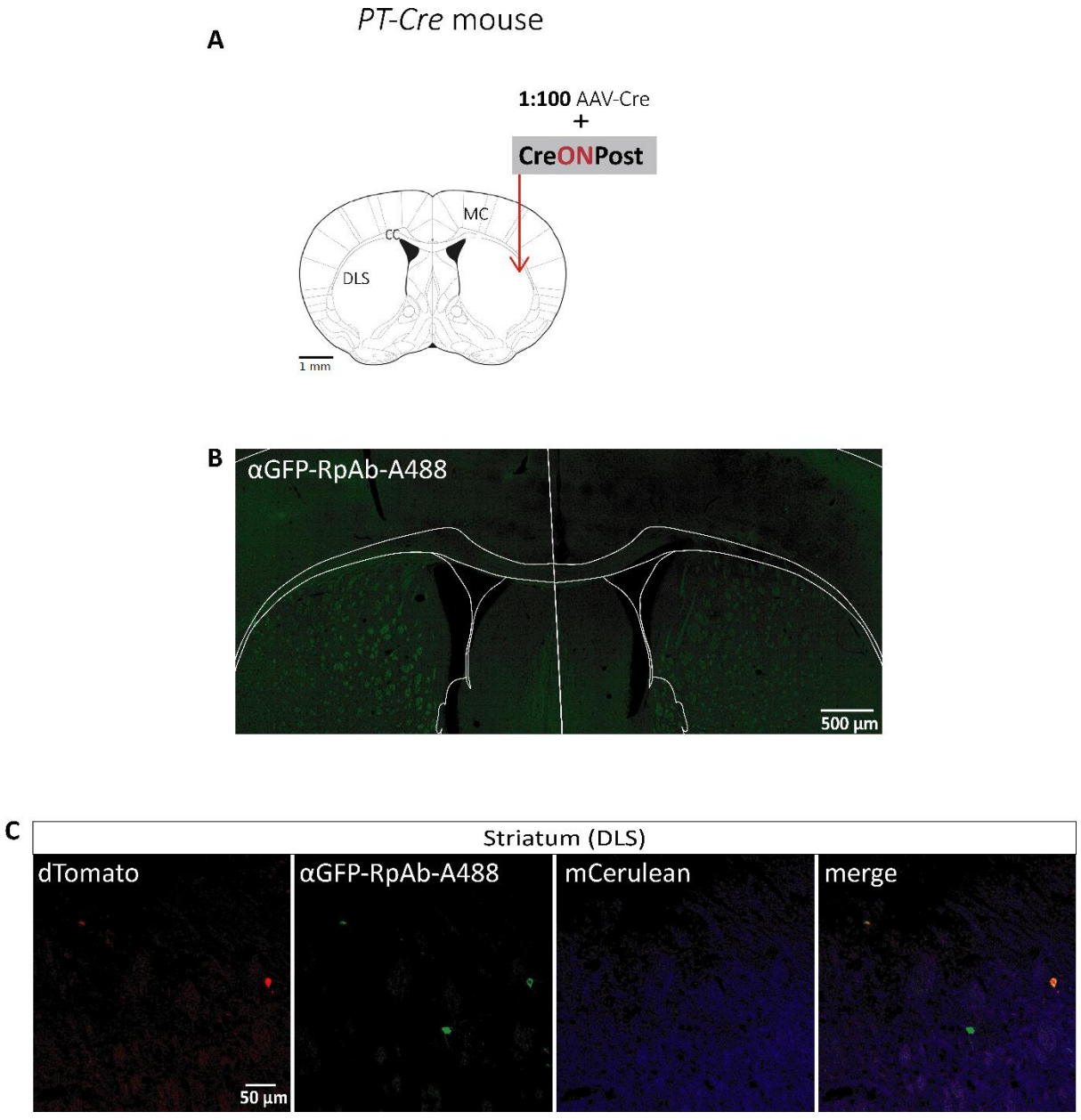

Figure 22 - Testing recognition of post-mGRASP by the rabbit polyclonal anti-GFP antibody conjugated with Alexa 488 using a PT-Cre mouse injected with only the post-mGRASP construct in the DLS. A, Schematic representation of the viral strategy (as detailed in the legend of Figure 7A). B, Representative single plane image (20x objective) of a brain slice immunolabelled against GFP using the rabbit polyclonal anti-GFP antibody conjugated with Alexa 488 (GFP-RpAb-A488) at 1:1000. C, Representative single plane images (20x objective) of dTomato, GFP and mCerulean signals in the in the DLS (n=1 mice). *CreONPost – AAV-ON-post-mGRASP-2A-dTomato, MC – motor cortex, CC – corpus callosum.*

2.3.3 – Immunolabelling against GFP with a mouse monoclonal antibody

We next used a mouse monoclonal anti-GFP antibody that was reported to be highly specific for the GFP reconstituted form, being unable to detect either split GFP halves alone[100]. We tested the ability of this antibody to enhance the mGRASP signal in brain slices from IT-Cre mice. Mice were injected with CreOFFPre (AAV-pre-mGRASP-mCerulean) in the MC and 1:100 AVV-Cre + CreONPost (AAV-ON-post-mGRASP-2A-dTomato) in the DLS (Figure 23A). As a monoclonal antibody, it only recognizes a specific epitope, and, therefore, we expected a higher signal-to-noise ratio. However, this antibody did not improve the detection of the reconstituted form (Figure 23B), as it showed heavy somatic labelling in the MC and extensive labelling of neurite-like structures in the DLS (Figure 23C,D). These results suggest that the mouse anti-GFP antibody recognizes the pre-mGRASP component. On the other hand, the antibody did not seem to recognize the post-mGRASP component, as indicated by the absence of green label in dTomato-positive cells (Figure 23D). Altogether, the specific reconstituted mGRASP signals did not improve, in contrary to what we predicted.

We performed an experiment to control for putative non-specific binding of the anti-mouse secondary antibody to the mouse tissue, using with the same experimental design as the previous experiment, but omitting the primary antibody incubation (Figure 24A). Notably, both the MC and the DLS presented strong green signals (Figure 24B-D). This result suggests that the mouse secondary antibody is recognizing mouse-specific epitopes in the brain tissue.

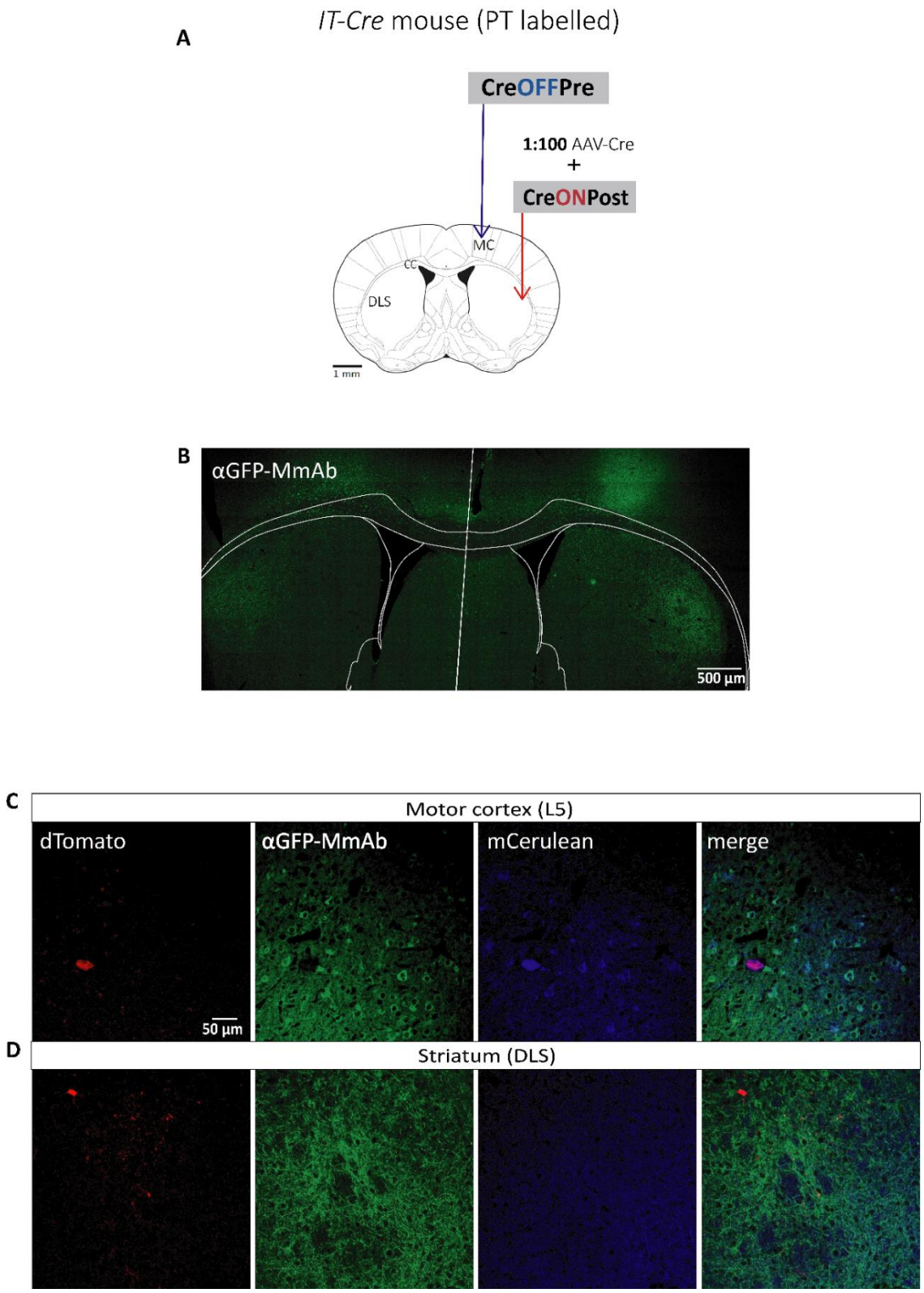

Figure 23 - Testing mGRASP signal amplification using a mouse monoclonal anti-GFP antibody in IT-Cre mice, expressing pre-mGRASP in PT neurons and post-mGRASP in striatal neurons. A, Schematic representation of the viral strategy (as detailed in the legend of figure 6A, except the AAV-Cre dilution that was 1:100 and the mice that were IT-Cre mice, i.e., pre-mGRASP will be expressed in PT neurons). B, Representative single plane image of a brain slice (20x objective) immunolabelled against GFP using a mouse monoclonal anti-GFP antibody (GFP-MmAb) at 1:500. C,D, Representative single plane images (20x objective) of dTomato, anti-GFP and

mCerulean signals in the motor cortex (MC) in C and DLS in D (n=1 mice). *CreOFFPre – AAV-OFF-pre-mGRASP-mCerulean, CreONPost – AAV-ON-post-mGRASP-2A-dTomato, CC – corpus callosum.*

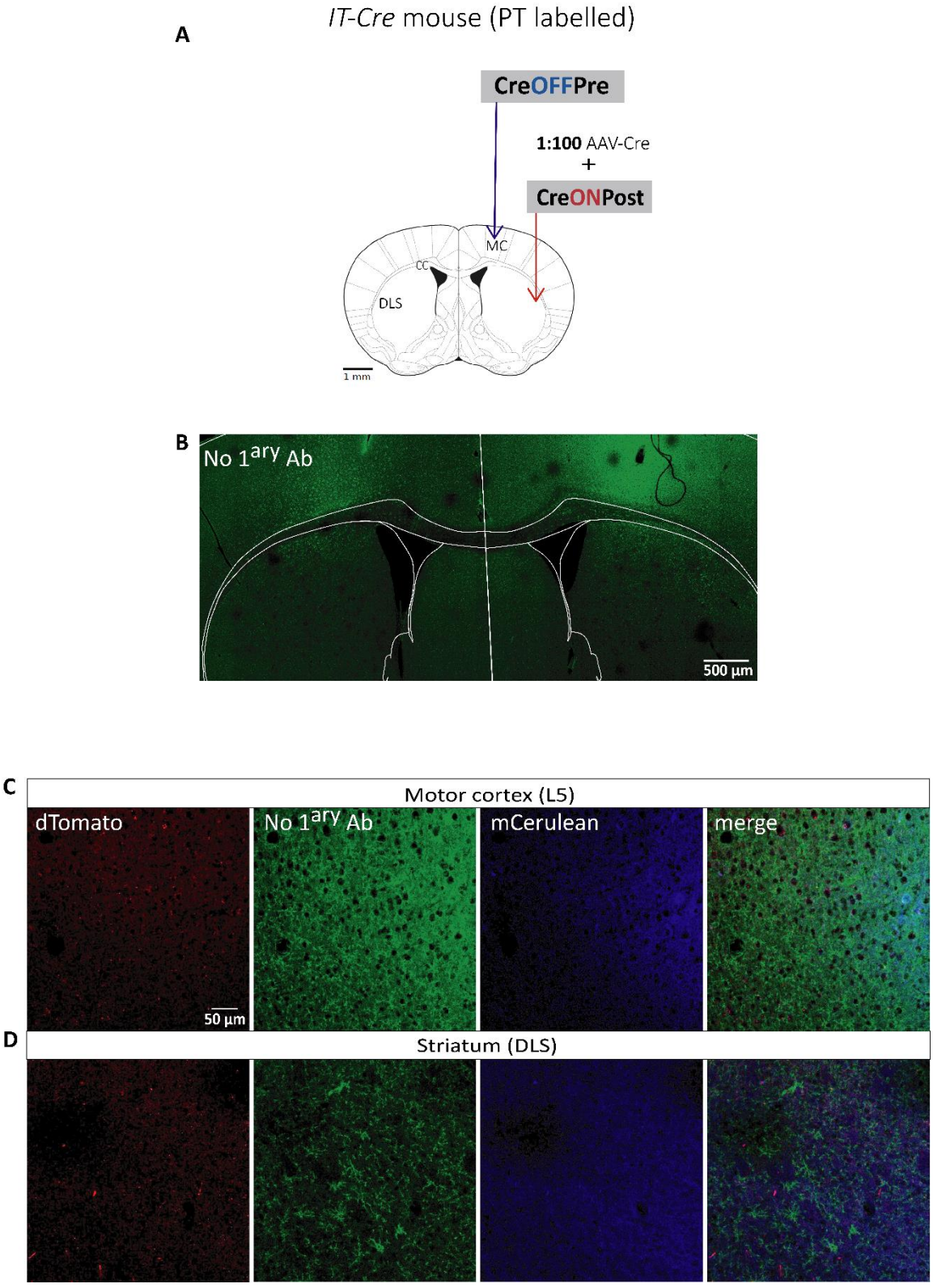

Figure 24 - Control immunolabelling experiment to assess non-specific binding of anti-mouse Alexa488 secondary antibody to mouse tissue, using IT-Cre mice expressing pre-mGRASP in PT neurons and post-mGRASP in striatal neurons. A, Schematic representation of the viral strategy (as detailed in the legend of figure

13A). B, Representative single plane image (20x objective) of a brain slice where incubation with primary antibody was omitted, keeping similar conditions for anti-mouse Alexa488 secondary antibody incubation as used for the immunostaining shown in Figure 13. C,D, Representative single plane images (20x objective) of dTomato, GFP and mCerulean signals in the motor cortex (MC) in C and DLS in D (n=1 mice), in the same slice as that shown in B. *CreOFFPre – AAV-OFF-pre-mGRASP-mCerulean, CreONPost – AAV-ON-post-mGRASP-2A-dTomato, CC – corpus callosum.*

To address this concern, we included an additional blocking agent in the immunolabelling protocol of the mouse monoclonal anti-GFP antibody, as to block endogenous mouse epitopes that could be recognized by the secondary antibody[94]: we added a mouse IgG (L+H) to the regular blocking solution (as detailed in the methods section) (Figure 25A). Under these conditions, the mouse anti-GFP antibody still revealed axon-like green signals in the DLS (Figure 25B), suggesting recognition of the pre-mGRASP component. Moreover, green labelling of dTomato-positive cell neurons in the DLS was again absent, confirming that the antibody did not recognize the post-mGRASP component (Figure 25B). The control experiment with mouse IgG blocking and no primary mouse anti-GFP antibody showed a dramatic reduction in green signal as compared to mouse IgG-untreated samples (Figure 25C). This suggests that blocking mouse epitopes with mouse IgG was efficient in clearing most of the unspecific signal, that resulted from the anti-mouse secondary antibody binding. However, since this antibody recognized the pre-mGRASP isoform, we were unable to amplify and validate specific mGRASP reconstitution in our experimental design.

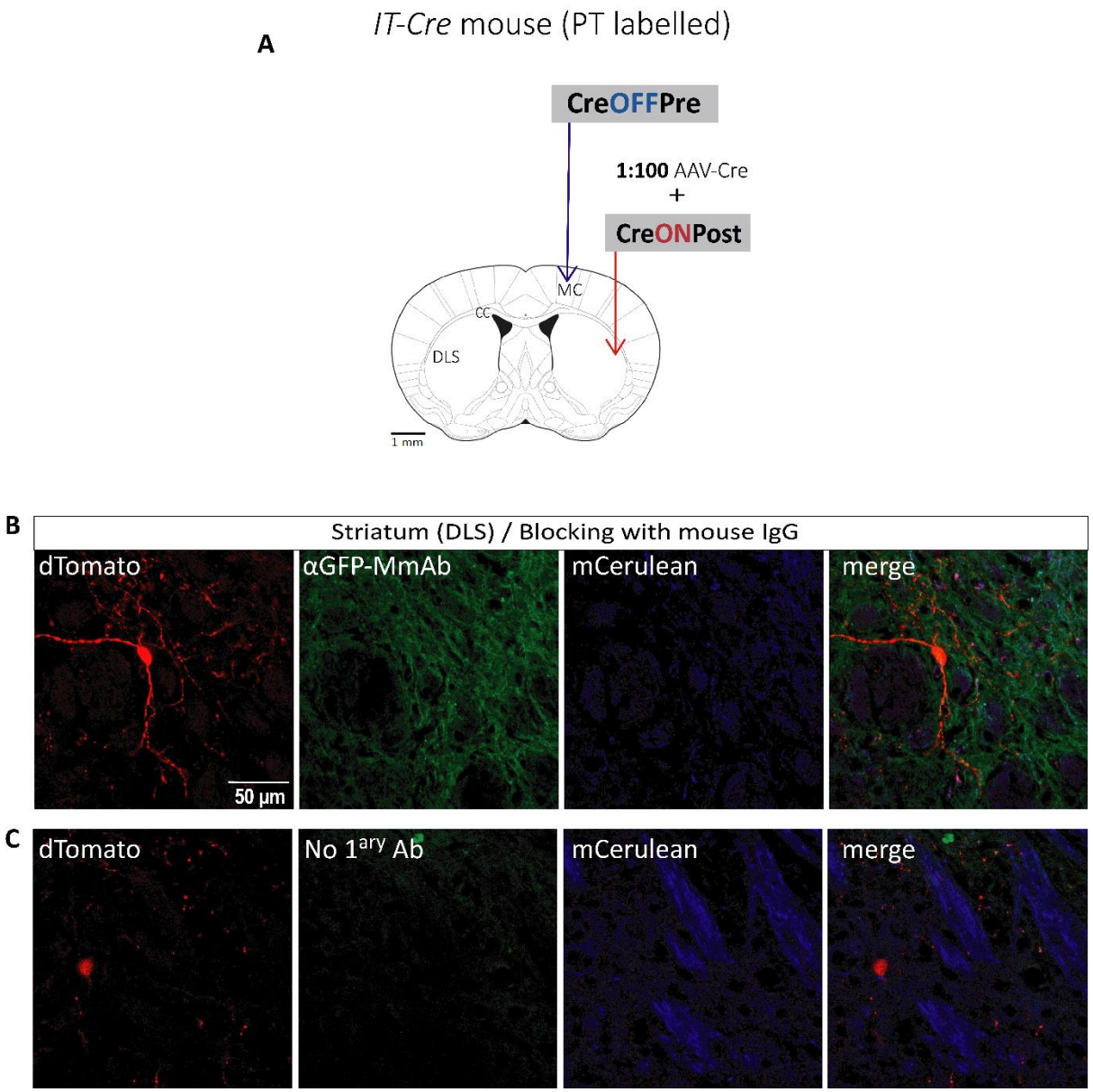

Figure 25 - Testing a blocking step with mouse IgG in the mGRASP signal amplification with the mouse monoclonal anti-GFP antibody, using IT-Cre mice expressing pre-mGRASP in PT neurons and post-mGRASP in striatal neurons. A - Schematic representation of the viral strategy (as detailed in the legend of figure 13A). B,C, Representative single plane images (20x objective) of dTomato, GFP and mCerulean signals in the DLS of a brain slice treated with a blocking step with mouse IgG, with (B) or without (C) incubation with the mouse monoclonal anti-GFP antibody (n=1 mice). *CreOFFPre – AAV-OFF-pre-mGRASP-mCerulean, CreONPost – AAV-ON-post-mGRASP-2A-dTomato, MC – motor cortex, CC – corpus callosum.*

In conclusion, although we found some puncta-like green signals in close apposition to dendritic structures of post-mGRASP-expressing neurons, we were unable to unequivocally identify corticostriatal synapses using mGRASP. It was not possible to discriminate between putative mGRASP signals and non-specific fluorescent signals in a convincing manner, despite testing different strategies to either amplify the mGRASP signal or reduce non-specific signals.

3. Morphological analysis of ChI and SPNs

Apart from the previously mentioned experimental tools, the mGRASP method is complemented with a set of digital tools that help analyse large amounts of imaging data[80,88,92,97,101,102]. One of the most relevant functions of this software is the automatized detection of synaptic contacts. For this purpose, the neuronal dendritic trees should be traced. To set up this tracing, we decided to first reconstruct neurons that were electrophysiologically recorded with whole-cell patch-clamp. This method requires the communication of the neuronal cytoplasm with a glass electrode containing an isosmotic solution, making it possible to deliver biocytin to individual neurons. Biocytin could be later revealed with Streptavidin conjugated with a fluorophore. The main reason for selecting these neurons to optimize dendritic reconstructions was the high signal to noise ratio in filled neurons, especially when compared with the weak dTomato signal expressed by post-mGRASP (Figure 16). Additionally, recorded neurons are few and usually sparse, further facilitating its tracing.

Since both SPNs and ChIs are putative targets of IT and PT corticostriatal inputs, we took advantage of slices where single ChIs and/or SPNs were filled and recorded for a functional study of these contacts in the DLS. This allowed us to troubleshoot the tracing method, aiming for future automatic mGRASP detection. At the same time, the reconstructed neurons provided useful information about the complexity of their dendrites, which would ultimately affect the integration of the inputs they receive.

We first confirmed the identity of putative ChIs using anti-ChAT labelling. In fact, all the neurons with electrophysiological properties compatible with ChIs (data not shown) were ChAT-positive, (12/12 ChI neurons, Figure 26). As expected, ChIs and SPNs were both labelled with streptavidin with high contrast (Figure 26A). Moreover, ChIs were easily identified and distinguished from SPNs by the ChAT staining (Figure 26B).

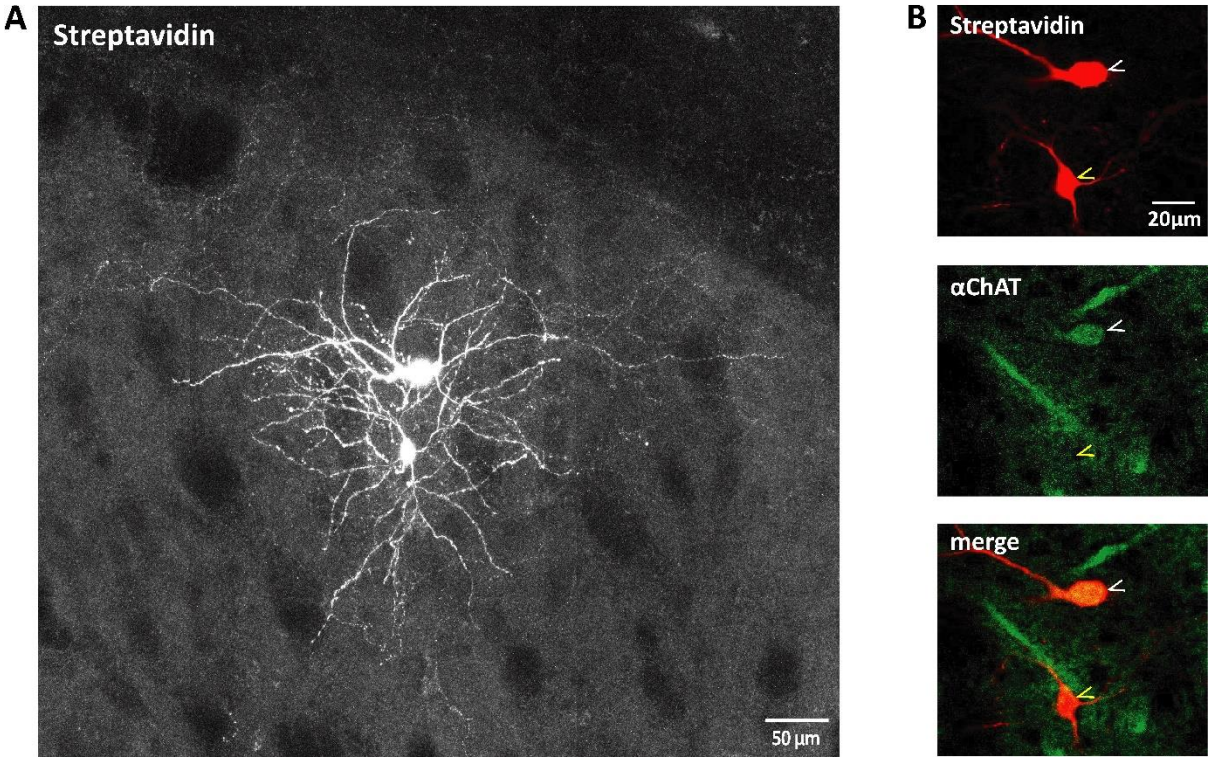

Figure 26 - Anti-ChAT and streptavidin immunolabelling of putative cholinergic (ChIs) and spiny projection neurons (SPNs), following electrophysiological recordings. A, Representative maximum intensity projection (MIP) of z-stack images (25x objective) showing a ChI-SPN pair in the DLS. Neurons were filled with biocytin and stained with streptavidin conjugated with Alexa 594. B, Example of MIPs of confocal image z-stacks (20x objective) showing a soma labelled with streptavidin in red and anti-ChAT antibody (αChAT) in green (white arrow) and another soma labelled with streptavidin in red and lacking the anti-ChAT label (yellow arrow). These neurons showed electrophysiological properties consistent with ChI (white arrow) and SPN (yellow arrow).

After confirming the identity of ChIs, our next focus was to study the dendritic tree complexity of both neuronal types. We reconstructed and obtained a skeleton of each neuronal dendritic tree using neuTube[80,81,88,102,103], the single neurite tracer plugin on FIJI/ImageJ[97] (Figure 27A and Figure 28A). For each reconstruction, a Sholl analysis was performed with FIJI/ImageJ[98] using a radius step size of 10 µm (Figure 27B). This analysis quantifies the number of dendrites that are intersected by each concentric circle, as exemplified in Figure 27C for the neurons reconstructed in Figure 27A.

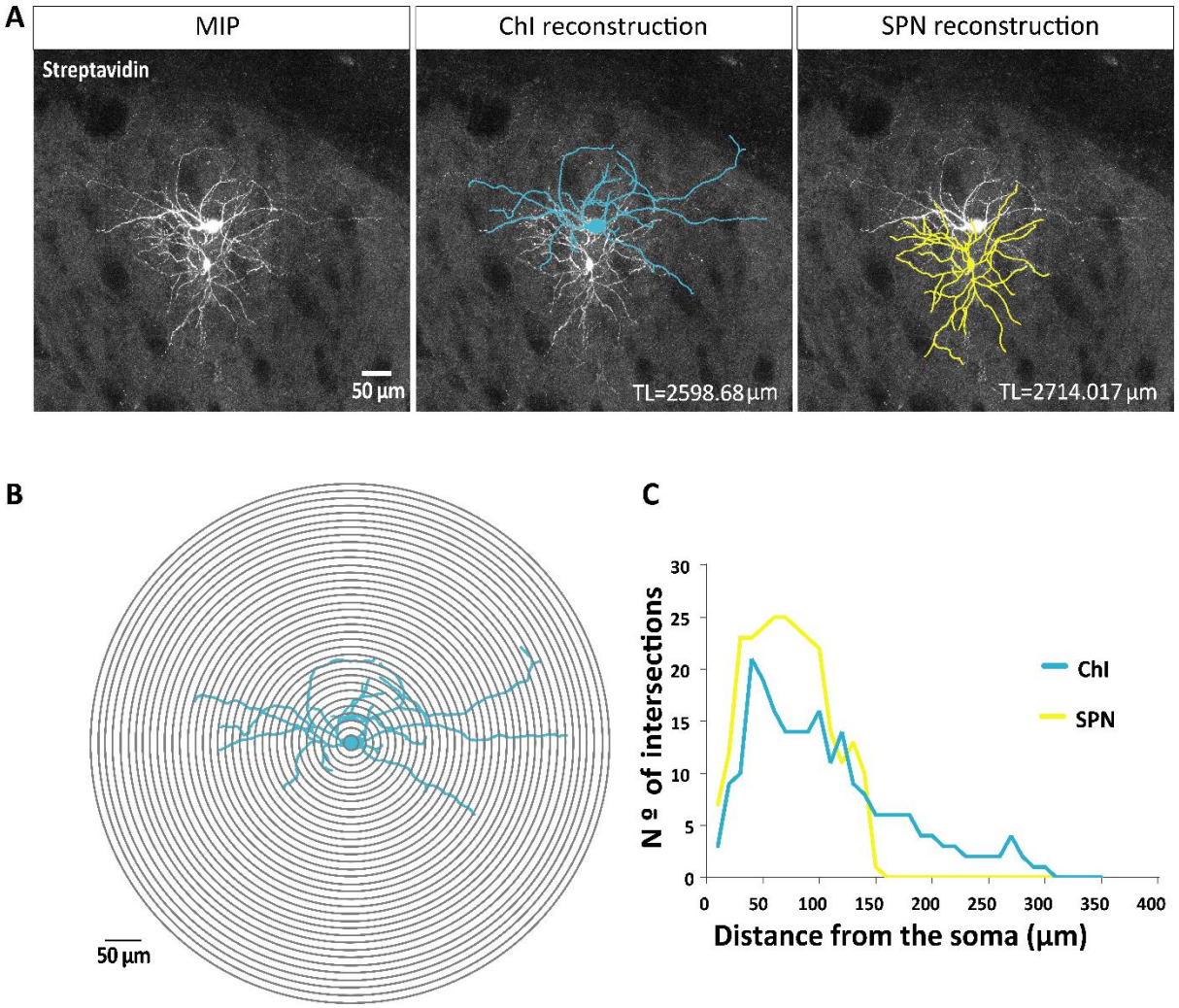

Figure 27 - Representative example of Sholl analysis profiles acquired from neurons recorded in the DLS. A, Example representation of the dendritic arbor reconstructions performed for both ChI and SPN neurons using z-stack images from a biocytin-streptavidin labelled brain slice. The MIP is represented on the left panel (see detailed description in the legend of Figure 16A). Middle panel, A reconstruction of a ChI (cyan) performed on the neuTube software was skeletonized and overlapped with the MIP image using Simple Neurite Tracer plugin (SNT) in FIJI/Image J. Right panel, Reconstruction of a neighboring SPN that was skeletonized and overlapped with the MIP image also using the neuTube software and SNT. The somas were filled after the reconstructions in Adobe Illustrator. B, Representation of the Sholl Analysis performed using as an example the ChI reconstruction shown in A. Radius step size was 10µm. The number of intersections between the reconstructed neuron and each concentric circle with a defined radius (i.e., distance from the soma) is summed and plotted for each neuron, as shown in C. C, Sholl Profile plot of the ChI and SPN neuron reconstructions represented in A. *TL – total dendritic length.*

At the population level, total dendritic length was not significantly different between SPNs and ChIs (mean ± s.e.m.: 2499 ± 188 µm, for n=5 SPNs; 2000 ± 241 µm, for n=12 ChIs; p=0.3284 by two-tailed Mann Whitney test). However, the dendrites of ChIs span a radius of

approximate 300 µm while SPN processes distribute along approximately half of that distance (Figure 28B). Altogether, these data show that the ChIs have sparser dendrites than SPNs, which may support their role within striatal microcircuits by increasing the likelihood of receiving diverse inputs[24]. This data shows a clear morphological distinction between the dendritic distribution of ChIs and SPNs.

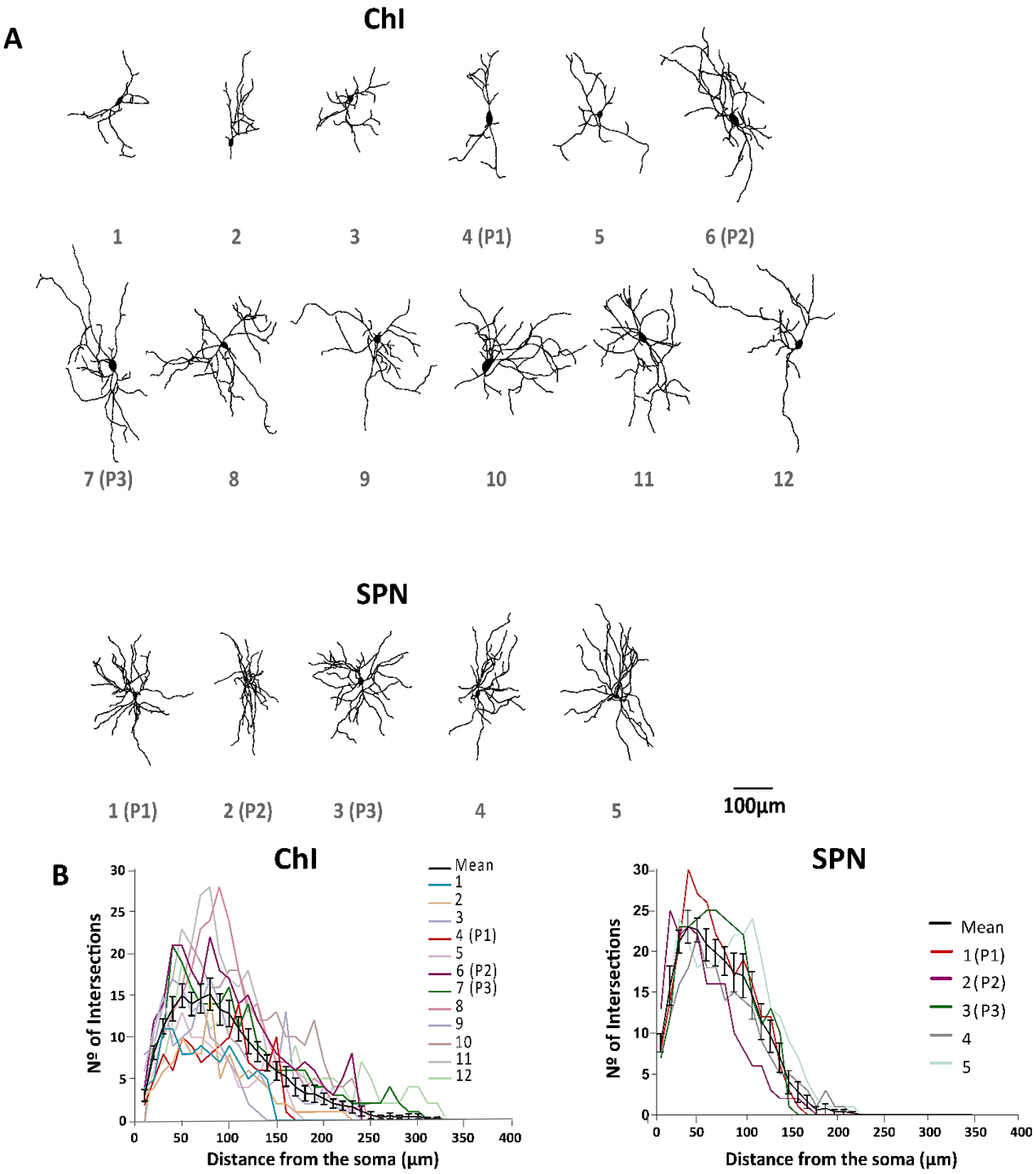

Figure 28 - Dendritic arbor reconstructions and corresponding Sholl analysis show morphological distinctions between recorded ChIs and SPNs. A, Dendritic reconstructions from all individual ChIs (n=12 neurons from 11 mice) and SPNs (n=5 neurons from 5 mice) analyzed. P1-3 represent pairs of neurons recorded on the same

slice. B, Population analysis of the dendritic distribution (Sholl) for ChI neurons (left), and SPNs (right), shown as mean number of intersections ± s.e.m as a function of the distance to the soma. Paired ChIs and SPNs are coded with the same line color.

Discussion and future perspectives

Corticostriatal synapses are the most important source of input to the striatum. Within this structure, SPNs integrate and compute, with additional modulation from interneurons and dopaminergic neurons, cortical and thalamic information that is then delivered to the output nuclei of the basal ganglia[9,22,24]. SPN morphological characteristics are tightly correlated with their function, as spine size and distance to the soma directly affect input integration[20,39,66,104,105]. However, the organization of corticostriatal contacts onto the different populations of SPNs has been difficult to tackle[9,52,59,60,106]. To better understand how SPNs collect and process IT and PT corticostriatal inputs, mapping of the distribution and density of these contacts needs to be resolved at the single synapse level[59,107,108]. The mGRASP technique was developed as a light microscopy-based anatomical approach to study synaptic connections by using trans-synaptic reconstitution of the GFP protein[80,81,86,87,100].

In this project, we aimed to establish the mGRASP technique to map long-range corticostriatal synapses onto SPNs and characterize their density and distribution. We used previously established protocols[80,92] to express pre-mGRASP in presynaptic PT and IT cortical neurons and post-mGRASP in postsynaptic SPNs. Our experimental design required optimization steps aiming to discriminate putative mGRASP signals from unspecific puncta-like fluorescent signals that were present in the samples (Figure 15). Nonetheless, throughout the extent of this project, we were neither able to reduce the non-specific fluorescent signals nor enhance the specific mGRASP signals. We believe that a combination of both technical and biological constrains limited mGRASP detection at corticostriatal synapses.

In parallel, we optimized neuronal tracing reconstructions as part of the effort to automatize synapse detection, as previously reported[80,81,92]. We efficiently reconstructed SPNs and ChIs, using neuTube tracing software together with FIJI/ImageJ for reconstruction analysis (Figure 27, 28), and found morphological differences between ChIs and SPNs at the level of dendritic distribution. ChIs modulate SPN activity, projecting throughout the striatum, and are therefore important regulators of striatal function[24,73,76,79]. As a future prospect, it would be interesting to study the striatal cholinergic microcircuitry in parallel to SPN input integration and computation analysis.

1. Connectivity constrains

In our study, we followed a very similar strategy to the one proposed to study hippocampal circuits with mGRASP[88,92]. However, studying long-range connectivity, and particularly

corticostriatal connections, may add additional challenges to the mGRASP synaptic analysis. Corticostriatal axons from any given cortical neuron are widely distributed across the striatum, minimizing the synaptic contacts they make with each postsynaptic SPN[3,6,45]. Thus, each SPN collects a unique set of inputs from a broad population of presynaptic partners, which reduces the probability of neighbouring neurons receiving the same input[40,58]. This can become an issue for mGRASP detection if cortical expression of pre-mGRASP is not wide-spread enough to label a significant fraction of the pre-synaptic partners to the post-mGRASP-labelled neuron analysed. Even more so in the case of IT contralateral projections, where axonal density is lower. It can also became specially problematic considering that each PT neuron has only a few collaterals in the ipsilateral striatum[3]. Moreover, cortical axons in the DLS do not seem to follow any specific spatial pattern[3,45,47], in contrast to layered structures such as cortex or hippocampus, where bundles of axonal fibres often run parallel to innervate neighbouring dendritic areas. In fact, previous mGRASP studies focused mainly on the hippocampus, where high synaptic density and a layered organization facilitated GFP reconstitution and detection. This is especially evident in the layers were pre-mGRASP expressing axons contact post-mGRASP expressing pyramidal cells[80,88,92].

In summary, both the sparseness of cortical inputs to SPNs and the lack of a clear spatial organization of corticostriatal axons are biological constrains that may have contributed to limit the detection of GFP reconstitution fluorescent signals in our study[3,45,58]. It is possible is that our gene delivery strategy might not have labelled enough presynaptic cortical cells innervating each post-mGRASP-expressing SPN. A potential future improvement to overcome sparse corticostriatal connectivity would be to perform multiple cortical injections at different AP and ML locations, to label more axons converging from different cortical areas into DLS. An additional improvement to enhance the likelihood of detecting mGRASP signals would be to amplify the dTomato signal using specific antibodies, as a means to improve the postsynaptic dendritic labelling and facilitate the detection of 'puncta-like' signals in close apposition to dendritic spines[88,92].

2. Methodological constrains

In addition to the biological constrains just described, our analysis was compromised by technical difficulties. Even though both the pre- and post-mGRASP components were being expressed in the pre- and postsynaptic cells, respectively (Figure 19, 20), the 'puncta-like' fluorescent signals that might have resulted from GFP reconstitution (Figure 15, white arrows) did not show a strong and easily detectable signal. This made it extremely difficult to distinguish the real mGRASP signals from non-specific fluorescent particles (Figure 15, yellow arrows), resulting in a very poor signal-to-noise ratio. In addition, some line-like signals that

result from unspecific expression of the mGRASP components were also detected in our samples (Figure 14)[81], which further compromised the detection of real mGRASP signals.

Although AAV-based gene delivery is efficient for expressing pre- and post-mGRASP components, the overexpression of mCherry, dTomato, mCerulean and split-GFP for long periods of time can affect several cellular maintenance systems and induce toxicity and/or immunogenicity[109]. To overcome this problem, sequential stereotaxic injections may reduce the possible toxic effects related to dTomato overexpression in SPNs, as this protein is more prone to misfold[31,32]. Since some pre-mGRASP constructs show long expression times, delaying the injection of the dTomato-expressing CreONPost AAV by one or two weeks could prevent misfolding and damage of cells expressing this protein[80].

We attempted a variety of different protocols to reduce noise from background fluorescent particles or to amplify specific mGRASP signals:

A) Protocols for reducing background noise

A glycine treatment of the sample tissue is advised in the original mGRASP protocol[80] to quench free aldehydes from the brain slices, thus reducing the autofluorescence of the samples. We tested this treatment aiming to reduce the background non-specific fluorescent signals. This treatment, however, was not successful in improving the signal-to-noise ratio (Figure 18). One possible alternative would be to increase either the washing step time and/or the number of washing steps or use the washing solution together with a low concentration of detergent, as to reduce non-specific antibody binding[110].

B) Immunostaining for boosting reconstituted GFP signals

Most antibodies that we used here have been previously tested in other GRASP systems[81,100], two of them being specific for the reconstituted GFP form in *Drosophila*[100]: the rabbit polyclonal and the mouse monoclonal anti-GFP antibodies. It is also worth mentioning that, to our knowledge, the mouse monoclonal anti-GFP antibody and the rabbit polyclonal anti-GFP antibody conjugated with Alexa 488 tested here, were never tested in mGRASP procedures in mammals before.

When we attempted to use the rabbit polyclonal anti-GFP antibody to amplify the mGRASP signal, we found that it recognized both pre- and post-mGRASP components (Figure 19, 20). This contrasted with the *Drosophila* study mentioned above[100] but is in agreement with other studies where this antibody was able to recognize post-mGRASP and confirm its expression in postsynaptic cells[88,92]. The rabbit polyclonal anti-GFP conjugated with Alexa 488 was also not specific for the reconstituted form of GFP, recognizing again both split-GFP isoforms (Figure 21, 22). Importantly, both antibodies detected pre- and post mGRASP in corticostriatal axons and striatal neurons, respectively, confirming that our experimental tools and procedures were efficient in expressing both split-GFP parts in the desired cells. Furthermore,

these data provides new evidence supporting that the mGRASP method is not specific for just one particular cell type[88].

In another attempt to detect the mGRASP signal, we tested the mouse monoclonal anti-GFP antibody[100]. Since we were using a mouse primary antibody in mouse tissue, we initially had a lot of background signal due to unspecific binding of the secondary anti-mouse antibody (Figure 23, 24). Adding a mouse IgG incubation as a blocking step[94] efficiently reduced fluorescent background signals (Figure 25B). Nonetheless, while post-mGRASP didn't seem to be recognized by this antibody (Figure 25A), we found that it recognized pre-mGRASP. Therefore, the mouse monoclonal anti-GFP antibody was also not selective for reconstituted GFP and, under the tested conditions, it cannot be used to amplify mGRASP signals in corticostriatal connections[100]. These results contradict a previous study in which this antibody was described as a being specific for the reconstituted GFP form in the fly[100]. In that report, the mouse monoclonal antibody only recognizes GFP when both the pre- and post-mGRASP isoforms are expressed in the pre and postsynaptic neurons, respectively[100]. No signal is detected when only one of the isoforms is present. However, in our study, we had clear recognition of the pre-mGRASP isoform in pre-synaptic cell bodies and axons (not shown and Figure 25A). The reasons for these discrepancies are unclear and may involve technical and/or biological constrains, such as lower antibody accessibility, suboptimal conformation of the pre-mGRASP protein epitope when it is not bound to the post-mGRASP isoform, specific matters related to their protocol or system.

In conclusion, none of the tested tools and protocols were able to amplify reconstituted GFP signals. The search for an antibody that recognizes reconstituted GFP specifically without binding to the pre or post-split-GFP forms would be one of the future directions for this project. However, based on the results obtained with the three antibodies we tested, two of them having been deemed specific for the mGRASP signal in other systems, we anticipate difficulties in finding a suitable antibody. A potential candidate would be a recently reported monoclonal antibody that seems to specifically bind to the GFP reconstituted form in the neuromuscular junction of *Drosophila* larvae[99].

C) Alternative strategies for mapping corticostriatal connections

One 'classical' strategy that could be approachable for this project would be an anatomical distribution analysis of pre and/or postsynaptic markers, such as Bassoon or Piccolo (pre), and PSD-95 (post)[82,111], together with pre and post-synaptic expression of fluorescent proteins (or biocytin filling) to reveal morphological anatomy. The main principle would be immunolabelling against a pre or post-synaptic marker in brain slices, showing AAV-mediated fluorescent protein expression, of IT or PT cortical axons and postsynaptic SPNs, allowing visualization of corticostriatal synaptic contacts[111–113]. The pre and postsynaptic selectivity and sparseness of labelling could rely on a combination of AAVs and Cre-transgenic animal lines[87],

similarly to what was used in this project. The colocalization of the synaptic marker with areas of close apposition between presynaptic and postsynaptic structures would indicate synaptic contacts between cortical neurons and a given SPN. This approach would rely on the development of robust criteria for automatic triple colocalization analysis but could be combined with the neuronal reconstruction methodology that we established in this project, to enable a study on the anatomical distribution of different inputs.

New techniques have also been developed alongside mGRASP to investigate synaptic contacts by light microscopy techniques. An example of this is array tomography, which uses several molecular markers in multiple rounds of immunolabeling, fluorescent tag bleaching and re-staining. Moreover, this technique combines confocal imaging and electron microscopy to achieve a better spatial resolution, by using ultrathin (50-200nm) or semithin (400-1000nm) brain slices[2,114]. This technique could be combined with the 'classical' immunostaining approach described above, to investigate with higher resolution IT and PT corticostriatal inputs to SPNs. However, by achieving a higher resolution, the scale at which we are focusing on is restrained by the sample size we can analyse under the electron microscope[80], therefore, this method would only allow the characterization of synaptic contacts at a single dendritic branch level[114]. To date, all the tools mentioned are still in process of optimization[2]. Regardless, the development of imaging techniques that allow the visualization of synaptic contacts can still add new prospects to other functional mapping methods. On the other hand, achieving functional connectomes of complex neural circuits is crucial to understand brain function and behaviour. Electrophysiology is a gold standard in the field to enable unequivocal determination of neuron-to-neuron functional connectivity and determination of dynamic properties at the single synapse level[115]. On the other hand, optogenetic techniques have been recently used to interrogate both short- and long-range circuits[95,115]. To achieve more precise functional maps, subcellular Channelrhodopsin-2 Assisted Circuit Mapping (sCRACM) is a method that allows the localization of functional monosynaptic contacts between specific presynaptic terminals within the dendritic tree of postsynaptic neurons[95,107,115]. It combines whole-cell recordings of postsynaptic neurons with photostimulation of axons from presynaptic neurons expressing Channelrhodopsin-2 (ChR2)[116]. For that, tetrodotoxin and 4-Aminopyridine are used to block action potential propagation along the axons, while maintaining presynaptic release, thus restricting neurotransmitter release only to the illuminated locations[95,107,115]. Using galvanometric mirrors (electromechanical device that deflects light beams using a mirror, projecting it onto a smaller scale spot than the regular beam), a blue laser beam activates ChR2 positive terminals in different spatial locations following a grid pattern, driving local neurotransmitter release near the postsynaptic neuron, which is being patched with an electrode. A map of the recorded postsynaptic currents evoked upon illumination can then be reported based on their amplitude, which correlates with the proximity to the stimulated axons[115,116]. Therefore,

sCRACM allows the spatial mapping of the synaptic contacts between defined neuronal populations expressing ChR2 and the specific cell-type of the postsynaptic patched neurons.

Nevertheless, a single cortical column in rodents, for example, has over 20,000 neurons processing thousands of synaptic inputs, which challenges precise circuit mapping[115]. Therefore, a combination of both anatomical mapping and functional analysis would be a better approach to understand how corticostriatal inputs are distributed and organized with single synapse resolution along SPN dendrites, and how those morphological characteristics correlate with input integration by SPNs.

References

1. Guo Q, Wang D, He X, et al. Whole-brain mapping of inputs to projection neurons and cholinergic interneurons in the dorsal striatum. *PLoS One*. 2015;10(4):1-15. doi:10.1371/journal.pone.0123381
2. Rah J-C, Feng L, Druckmann S, Lee H, Kim J. From a meso- to micro-scale connectome: array tomography and mGRASP. *Front Neuroanat*. 2015;9(June):1-12. doi:10.3389/fnana.2015.00078
3. Hooks BM, Papale AE, Paletzki RF, et al. Topographic precision in sensory and motor corticostriatal projections varies across cell type and cortical area. *Nat Commun*. 2018;9(1). doi:10.1038/s41467-018-05780-7
4. Matamales M, Götz J, Bertran-Gonzalez J. Quantitative imaging of cholinergic interneurons reveals a distinctive spatial organization and a functional gradient across the mouse striatum. *PLoS One*. 2016;11(6):1-13. doi:10.1371/journal.pone.0157682
5. Balleine BW, Liljeholm M, Ostlund SB. The integrative function of the basal ganglia in instrumental conditioning. *Behav Brain Res*. 2009;199(1):43-52. doi:10.1016/j.bbr.2008.10.034
6. Gerfen CR, Bolam JP, Gerfen CR, Bolam JP. The Neuroanatomical Organization of the Basal Ganglia. In: Steiner H, Tseng KY, eds. *Handbook of Basal Ganglia Structure and Function*. 1st ed. Chicago, USA: Academic Press, Elsevier; 2010:3-28. doi:10.1016/B978-0-12-374767-9.00001-9
7. Huerta-Ocampo I, Mena-Segovia J, Bolam JP. Convergence of cortical and thalamic input to direct and indirect pathway medium spiny neurons in the striatum. *Brain Struct Funct*. 2014;219(5):1787-1800. doi:10.1007/s00429-013-0601-z
8. Hunnicutt BJ, Jongbloets BC, Birdsong WT, Gertz KJ, Zhong H, Mao T. A comprehensive excitatory input map of the striatum reveals novel functional organization. *Elife*. 2016;5(November2016):1-32. doi:10.7554/eLife.19103
9. Shepherd GMG. Corticostriatal connectivity and its role in disease. *Nat Rev Neurosci*. 2013;14(4):278-291. doi:10.1038/nrn3469
10. DeLong MR, Wichmann T. Circuits and circuit disorders of the basal ganglia. *Arch Neurol*. 2007;64(1):20-24. doi:10.1001/archneur.64.1.20
11. Li CX, Waters RS. Organization of the mouse motor cortex studied by retrograde tracing and intracortical microstimulation (ICMS) mapping. *Can J Neurol Sci*. 1991;18(1):28-38. http://www.ncbi.nlm.nih.gov/pubmed/2036613. Accessed September 13, 2018.
12. Dr. K. Brodmann. *Brodmann's Localisation in the Cerebral Cortex: The Principles of Comparative Localisation in the Cerebral Cortex Based on Cytoarchitectonics*. (Garey LJ, ed.). Springer; 2006.
13. Wong AL, Haith AM, Krakauer JW. Motor planning. *Neurosci*. 2015;21(4):385-398. doi:10.1177/1073858414541484
14. Campbell AW. *Histological Studies on the Localization of Cerebral Function*. Archived f. Cambridge, MA: Cambridge University Press; 1905.
15. Motor Cortex (Section 3, Chapter 3) Neuroscience Online: An Electronic Textbook for the

Neurosciences | Department of Neurobiology and Anatomy - The University of Texas Medical School at Houston. https://nba.uth.tmc.edu/neuroscience/m/s3/chapter03.html. Accessed September 13, 2018.

16. Jones EG. *The Thalamus*. Cambridge University Press; 2007. http://admin.cambridge.org/academic/subjects/life-sciences/neuroscience/thalamus-2nd-edition?format=WX. Accessed September 13, 2018.

17. Alloway KD, Smith JB, Mowery TM, Watson GDR. Sensory Processing in the Dorsolateral Striatum: The Contribution of Thalamostriatal Pathways. *Front Syst Neurosci*. 2017;11(July):1-19. doi:10.3389/fnsys.2017.00053

18. Smith Y, Galvan A, Ellender TJ, et al. The thalamostriatal system in normal and diseased states. *Front Syst Neurosci*. 2014;8(January):1-18. doi:10.3389/fnsys.2014.00005

19. Kemp JM, Powell TPS. The structure of the caudate nucleus of the cat: light and electron microscopy. *Philos Trans R Soc B*. 1971;262(845):383-401.

20. Plenz D, Wickens JR. The Striatal Skeleton: Medium Spiny Projection Neurons and their Lateral Connections. In: Steiner H, Tseng KY, eds. *Handbook of Basal Ganglia Structure and Function*. 1st ed. Chicago, USA: Academic Press, Elsevier; 2010:99-112.

21. Lapper SR, Bolam JP. Input from the frontal cortex and the parafascicular nucleus to cholinergic interneurons in the dorsal striatum of the rat. *Neuroscience*. 1992;51(3):533-545. doi:10.1016/0306-4522(92)90293-B

22. Kreitzer AC, Malenka RC. Striatal plasticity and basal ganglia circuit function. *Neuron*. 2008;60(4):543-554. doi:10.1016/j.neuron.2008.11.005

23. Assous M, Tepper JM. Excitatory extrinsic afferents to striatal interneurons and interactions with striatal microcircuitry. *Eur J Neurosci*. 2018;(February):1-11. doi:10.1111/ejn.13881

24. Abudukeyoumu N, Hernandez-Flores T, Garcia-Munoz M, Arbuthnott GW. Cholinergic modulation of striatal microcircuits. *Eur J Neurosci*. 2019;49(5):604-622. doi:10.1111/ejn.13949

25. Redgrave P, Rodriguez M, Smith Y, Rodriguez-oroz MC. Goal-directed and habitual control in the basal ganglia: implications for Parkinson's disease. *Nat Publ Gr*. 2010;11(11):760-772. doi:10.1038/nrn2915.Goal-directed

26. Lee J. Decisions, Decisions: The Neurobiology of the effects of Dopamine Replacement Therapy on Decision-Making in Parkinson's Disease. *J Eur Psychol Students*. 2015;6(1):45-52. doi:10.5334/jeps.cv

27. Bahuguna J, Aertsen A, Kumar A. Existence and Control of Go/No-Go Decision Transition Threshold in the Striatum. *PLoS Comput Biol*. 2015;11(4):1-35. doi:10.1371/journal.pcbi.1004233

28. Ferreira-Pinto MJ, Ruder L, Capelli P, Arber S. Connecting Circuits for Supraspinal Control of Locomotion. *Neuron*. 2018;100(2):361-374. doi:10.1016/j.neuron.2018.09.015

29. Kreitzer AC, Malenka RC. Endocannabinoid-mediated rescue of striatal LTD and motor deficits in Parkinson's disease models. *Nature*. 2007;445(7128):643-647. doi:10.1038/nature05506

30. Plotkin JL, Surmeier DJ. Corticostriatal synaptic adaptations in Huntington's disease. *Curr Opin Neurobiol*. 2015;33:53-62. doi:10.1016/j.conb.2015.01.020

31. Da Cunha C, Boschen SL, Gómez-a A, et al. Toward sophisiticated basal ganglia

neuromodulation: review on basal gaglia deep brain stimulation. *Neurosci Biobehav Rev*. 2015;58:186-210. doi:10.1016/j.neubiorev.2015.02.003.Toward

32. Cui G, Jun SB, Jin X, et al. Concurrent Activation of Striatal Direct and Indirect Pathways During Action Initiation. *Nature*. 2013;494(7436):238-242. doi:10.1038/nature11846.Concurrent
33. Tecuapetla F, Matias S, Dugue GP, Mainen ZF, Costa RM. Balanced activity in basal ganglia projection pathways is critical for contraversive movements. *Nat Commun*. 2014;5:1-10. doi:10.1038/ncomms5315
34. Klaus A, Martins GJ, Paixao VB, Zhou P, Paninski L, Costa RM. The Spatiotemporal Organization of the Striatum Encodes Action Space. *Neuron*. 2017;95(5):1171-1180.e7. doi:10.1016/j.neuron.2017.08.015
35. Tecuapetla F, Jin X, Lima SQ, Costa RM. Complementary Contributions of Striatal Projection Pathways to Action Initiation and Execution. *Cell*. 2016;166(3):703-715. doi:10.1016/j.cell.2016.06.032
36. Barbera G, Liang B, Zhang L, et al. Spatially Compact Neural Clusters in the Dorsal Striatum Encode Locomotion Relevant Information. *Neuron*. 2016;92(1):202-213. doi:10.1016/j.neuron.2016.08.037
37. Isomura Y, Takekawa T, Harukuni R, et al. Reward-modulated motor information in identified striatum neurons. *J Neurosci*. 2013;33(25):10209-10220. doi:10.1523/JNEUROSCI.0381-13.2013
38. Surmeier DJ, Ding J, Day M, Wang Z, Shen W. D1 and D2 dopamine-receptor modulation of striatal glutamatergic signaling in striatal medium spiny neurons. *Trends Neurosci*. 2007;30(5):228-235. doi:10.1016/J.TINS.2007.03.008
39. Plotkin JL, Day M, Surmeier DJ. Synaptically driven state transitions in distal dendrites of striatal spiny neurons. *Nat Neurosci*. 2011;14(7):881-888. doi:10.1038/nn.2848
40. Wickens JR, Arbuthnott GW. Gating of Cortical Input to the Striatum. In: Steiner H, Tseng KY, eds. *Handbook of Basal Ganglia Structure and Function*. 1st ed. Chicago, USA: Academic Press, Elsevier; 2010:341-351.
41. Calabresi P, Picconi B, Tozzi A, Ghiglieri V, Di Filippo M. Direct and indirect pathways of basal ganglia: A critical reappraisal. *Nat Neurosci*. 2014;17(8):1022-1030. doi:10.1038/nn.3743
42. Alexander G, DeLong MR, Strick PL. Parallel Organization of Functionally Segregated Circuits Linking Basal Ganglia and Cortex. *Annu Rev Neurosci*. 1986;9(1):357-381. doi:10.1146/annurev.neuro.9.1.357
43. Kravitz A V., Freeze BS, Parker PRL, et al. Regulation of parkinsonian motor behaviours by optogenetic control of basal ganglia circuitry. *Nature*. 2010;466(7306):622-626. doi:10.1038/nature09159
44. Sharott A, Vinciati F, Nakamura KC, Magill PJ. A population of indirect pathway striatal projection neurons is selectively entrained to parkinsonian beta oscillations. *J Neurosci*. 2017;37(41):0658-17. doi:10.1523/JNEUROSCI.0658-17.2017
45. Zheng T, Wilson CJ. Corticostriatal Combinatorics: The Implications of Corticostriatal Axonal Arborizations. *J Neurophysiol*. 2002;87(2):1007-1017. doi:10.1152/jn.00519.2001
46. Reiner A. Corticostriatal projection neurons – dichotomous types and dichotomous functions.

Front Neuroanat. 2010;4(October):1-15. doi:10.3389/fnana.2010.00142

47. Hintiryan H, Foster NN, Bowman I, et al. The mouse cortico-striatal projectome. *Nat Neurosci*. 2016;19(8):1100-1114. doi:10.1038/nn.4332

48. Lévesque M, Charara A, Gagnon S, Parent A, Deschênes M. Corticostriatal projections from layer V cells in rat are collaterals of long-range corticofugal axons. *Brain Res*. 1996;709(2):311-315. doi:10.1016/0006-8993(95)01333-4

49. Fame RM, Macdonald JL, Macklis JD. Development, Specification, and Diversity of Callosal Projection Neurons. *Trends Neurosci*. 2011;34(1):41-50. doi:10.1038/jid.2014.371

50. Reiner A, Jiao Y, Del Mar N, Laverghetta AV, Lei WL. Differential morphology of pyramidal tract-type and intratelencephalically projecting-type corticostriatal neurons and their intrastriatal terminals in rats. *J Comp Neurol*. 2003;457(4):420-440. doi:10.1002/cne.10541

51. Reiner A. Organization of Corticostriatal Projection Neuron types. In: Steiner H, Tseng KY, eds. *Handbook of Basal Ganglia Structure and Function*. 20th ed. Chicago, USA: Academic Press, Elsevier; 2010:323-339.

52. Kress GJ, Yamawaki N, Wokosin DL, Wickersham IR, Shepherd GMGG, Surmeier DJ. Convergent cortical innervation of striatal projection neurons. *Nat Neurosci*. 2013;16(6):665-667. doi:10.1038/nn.3397

53. Oorschot DE. Cell Types in the Different Nuclei of the Basal Ganglia. In: Steiner H, Tseng KY, eds. *Handbook of Basal Ganglia Structure and Function*. 1st ed. Chicago, USA: Academic Press, Elsevier; 2010:63-74.

54. Reig R, Silberberg G. Distinct corticostriatal and intracortical pathways mediate bilateral sensory responses in the striatum. *Cereb Cortex*. 2016;26(12):4405-4415. doi:10.1093/cercor/bhw268

55. Suter BA, Migliore M, Shepherd GMG. Intrinsic electrophysiology of mouse corticospinal neurons: A class-specific triad of spike-related properties. *Cereb Cortex*. 2013;23(8):1965-1977. doi:10.1093/cercor/bhs184

56. Fujiyama F, Sohn J, Nakano T, et al. Exclusive and common targets of neostriatofugal projections of rat striosome neurons: A single neuron-tracing study using a viral vector. *Eur J Neurosci*. 2011;33(4):668-677. doi:10.1111/j.1460-9568.2010.07564.x

57. Shipp S. The functional logic of corticostriatal connections. *Brain Struct Funct*. 2017;222(2):669-706. doi:10.1007/s00429-016-1250-9

58. Wilson CJ. Striatal circuitry: Categorically selective, or selectively categorical? In: Miller R, Wickens J, eds. *Brain Dynamics and the Striatal Complex*. 2nd ed. Otago, New Zeland: CRC Press; 2000:289-305.

59. Morita K. Differential cortical activation of the striatal direct and indirect pathway cells: reconciling the anatomical and optogenetic results by using a computational method. *J Neurophysiol*. 2014;112(1):120-146. doi:10.1152/jn.00625.2013

60. Lei W, Jiao. Evidence for Differential Cortical Input to Direct Pathway versus Indirect Pathway Striatal Projection Neurons in Rats. *J Neurosci*. 2004;24(38):8289-8299. doi:10.1523/JNEUROSCI.1990-04.2004

61. Cepeda C, André VM, Yamazaki I, Wu N, Kleiman-Weiner M, Levine MS. Differential electrophysiological properties of dopamine D1 and D2 receptor-containing striatal medium-sized spiny neurons. *Eur J Neurosci*. 2008;27(3):671-682. doi:10.1111/j.1460-9568.2008.06038.x

62. Lee T, Kaneko T, Taki K, Mizuno N. Preprodynorphin-, Preproenkephalin-, and Preprotachykinin-Expressing Neurons in the Rat Neostriatum : An Analysis by Immunocytochemistry and Retrograde Tracing. *J Comp Neurol*. 1997;386(February):229-244.

63. Al-muhtasib N, Forcelli PA, Vicini S. Differential electrophysiological properties of D1 and D2 spiny projection neurons in the mouse nucleus accumbens core. *Physiol Rep*. 2018;6(13):e13784. doi:10.14814/phy2.13784

64. Murer MG, O'Donnell P. Gating of Cortical Input Through the Striatum. In: Steiner H, Tseng KY, eds. *Handbook of Basal Ganglia Structure and Function*. 1st ed. Chicago, USA: Academic Press, Elsevier; 2010:341-351. doi:10.1016/B978-0-12-802206-1.00022-2

65. Nisenbaum E, Wilson C. Potassium currents responsible for inward and outward rectification in rat neostriatal spiny projection neurons. *J Neurosci*. 1995;15(6):4449-4463. doi:10.1523/jneurosci.15-06-04449.1995

66. Antic SD, Hines M, Lytton WW. Embedded ensemble encoding hypothesis: The role of the "Prepared" cell. *J Neurosci Res*. 2018;(March):1-17. doi:10.1002/jnr.24240

67. Bouyer JJ, Park DH, Joh TH, Pickel VM. Chemical and structural analysis of the relation between cortical inputs and tyrosine hydroxylase-containing terminals in rat neostriatum. *Brain Res*. 1984;302(2):267-275. doi:10.1016/0006-8993(84)90239-7

68. Freund TF, Powell JF, Smith AD. Tyrosine hydroxylase-immunoreactive boutons in synaptic contact with identified striatonigral neurons, with particular reference to dendritic spines. *Neuroscience*. 1984;13(4):1189-1215. doi:10.1016/0306-4522(84)90294-X

69. Yust R. Structure of Spines. In: *Dendritic Spines*. Cambridge, Massachusetts, London, England: The MIT Press; 2010:95-108. doi:10.1016/B978-0-12-397267-5.00145-X

70. Bennett BD, Bolam JP. Synaptic input and output of parvalbumin-immunoreactive neurons in the neostriatum of the rat. *Neuroscience*. 1994;62(3):707-719. doi:10.1016/0306-4522(94)90471-5

71. Bolam JP, Wainer BH, Smith AD. Characterization of cholinergic neurons in the rat neostriatum. A combination of choline acetyltransferase immunocytochemistry, Golgi-impregnation and electron microscopy. *Neuroscience*. 1984;12(3):711-718. doi:10.1016/0306-4522(84)90165-9

72. Bolam JP, Hanley JJ, Booth PAC, Bevan MD. Synaptic organisation of the basal ganglia. *J Anat*. 2000;196:527-542.

73. Lim SAO, Kang UJ, McGehee DS. Striatal cholinergic interneuron regulation and circuit effects. *Front Synaptic Neurosci*. 2014;6(SEP):1-23. doi:10.3389/fnsyn.2014.00022

74. Goldberg JA, Wilson CJ. The Cholinergic Interneurons of the Striatum: Intrinsic Properties Underlie Multiple Discharge Patterns. In: Steiner H, Tseng KY, eds. *Handbook of Basal Ganglia Structure and Function*. 1st ed. Chicago, USA: Academic Press, Elsevier; 2010:133-149.

75. Kawaguchi Y, Wilson CJ, Augood SJ, Emson PC. Striatal interneurones: chemical, physiological

and morphological characterization. *Trends Neurosci*. 1995;18(12):527-535.

76. Zhou FM, Wilson CJ, Dani JA. Cholinergic interneuron characteristics and nicotinic properties in the striatum. *J Neurobiol*. 2002;53(4):590-605. doi:10.1002/neu.10150

77. Gonzales KK, Smith Y. Striatal Cholinergic interneurons in the dorsal and ventral striatum: anatomical and functional considerations in normal and diseased conditions. *Annu New York Acad Sci*. 2015;1349(1):1-45. doi:110.1016/j.bbi.2017.04.008

78. Deffains M, Bergman H. Striatal cholinergic interneurons and cortico-striatal synaptic plasticity in health and disease. *Mov Disord*. 2015;30(8):1014-1025. doi:10.1002/mds.26300

79. Aosaki T, Miura M, Suzuki T, Nishimura K, Masuda M. Acetylcholine-dopamine balance hypothesis in the striatum: An update. *Geriatr Gerontol Int*. 2010;10(SUPPL. 1):S148-S157. doi:10.1111/j.1447-0594.2010.00588.x

80. Feng L, Kwon O, Lee B, Oh WC, Kim J. Using mammalian GFP reconstitution across synaptic partners (mGRASP) to map synaptic connectivity in the mouse brain. *Nat Protoc*. 2014. doi:10.1038/nprot.2014.166

81. Kim J, Zhao T, Petralia RS, et al. MGRASP enables mapping mammalian synaptic connectivity with light microscopy. *Nat Methods*. 2012;9(1):96-102. doi:10.1038/nmeth.1784

82. Dzyubenko E, Rozenberg A, Hermann DM, Faissner A. Colocalization of synapse marker proteins evaluated by STED-microscopy reveals patterns of neuronal synapse distribution in vitro. *J Neurosci Methods*. 2016;273:149-159. doi:10.1016/j.jneumeth.2016.09.001

83. Bock DD, Lee WCA, Kerlin AM, et al. Network anatomy and in vivo physiology of visual cortical neurons. *Nature*. 2011;471(7337):177-184. doi:10.1038/nature09802

84. Cai D, Cohen KB, Luo T, Lichtman JW, Sanes JR. New Tools for the Brainbow Toolbox. *Nat Methods*. 2013;10(6):540-547. doi:10.1038/nmeth.2450.NEW

85. Lerner TN, Ye L, Deisseroth K. Communication in Neural Circuits: Tools, Opportunities, and Challenges. *Cell*. 2016;164(6):1136-1150. doi:10.1016/j.cell.2016.02.027

86. Feinberg EH, VanHoven MK, Bendesky A, et al. GFP Reconstitution Across Synaptic Partners (GRASP) Defines Cell Contacts and Synapses in Living Nervous Systems. *Neuron*. 2008;57(3):353-363. doi:10.1016/j.neuron.2007.11.030

87. Yamagata M, Sanes JR. Transgenic strategy for identifying synaptic connections in mice by fluorescence complementation (GRASP). *Front Mol Neurosci*. 2012;5(February):1-9. doi:10.3389/fnmol.2012.00018

88. Kwon O, Feng L, Druckmann S, Kim J. Schaffer Collateral Inputs to CA1 Excitatory and Inhibitory Neurons Follow Different Connectivity Rules. *J Neurosci*. 2018. doi:10.1523/JNEUROSCI.0155-18.2018

89. Ghosh I, Hamilton AD, Regan L. Antiparallel leucine zipper-directed protein reassembly: Application to the green fluorescent protein [12]. *J Am Chem Soc*. 2000;122(23):5658-5659. doi:10.1021/ja994421w

90. Romei MG, Boxer SG. Split Green Fluorescent Proteins : Scope , Limitations , and Outlook. 2019:19-44.

91. Kent KP, Childs W, Boxer SG. Deconstructing green fluorescent protein. *J Am Chem Soc*.

2008;130(30):9664-9665. doi:10.1021/ja803782x

92. Druckmann S, Feng L, Lee B, et al. Structured Synaptic Connectivity between Hippocampal Regions. *Neuron*. 2014;81(3):629-640. doi:10.1016/j.neuron.2013.11.026

93. Bäck S, Dossat A, Parkkinen I, et al. Neuronal Activation Stimulates Cytomegalovirus Promoter-Driven Transgene Expression. *Mol Ther - Methods Clin Dev*. 2019;14(September):180-188. doi:10.1016/j.omtm.2019.06.006

94. Abcam. Mouse on Mouse (MOM) staining Procedure.

95. Morgenstern NA, Bourg J, Petreanu L. Multilaminar networks of cortical neurons integrate common inputs from sensory thalamus. *Nat Neurosci*. 2016;19(8):1034-1040. doi:10.1038/nn.4339

96. Preibisch S, Saalfeld S, Tomancak P. Globally optimal stitching of tiled 3D microscopic image acquisitions. *Bioinformatics*. 2009;25(11):1463-1465. doi:10.1093/bioinformatics/btp184

97. Longair MH, Baker DA, Armstrong JD. Simple neurite tracer: Open source software for reconstruction, visualization and analysis of neuronal processes. *Bioinformatics*. 2011;27(17):2453-2454. doi:10.1093/bioinformatics/btr390

98. Ferreira TA, Blackman A V., Oyrer J, et al. Neuronal morphometry directly from bitmap images. *Nat Methods*. 2014;11(10):982-984. doi:10.1038/nmeth.3125

99. Shearin HK, Quinn CD, Mackin RD, Macdonald IS, Stowers RS. t-GRASP, a targeted GRASP for assessing neuronal connectivity. *J Neurosci Methods*. 2018;306(January):94-102. doi:10.1016/j.jneumeth.2018.05.014

100. Gordon MD, Scott K. Motor control in a Drosophila taste circuit. *Neuron*. 2009;61(3):373-384. doi:10.1016/j.neuron.2008.12.033.Motor

101. Kayasandik C, Negi P, Laezza F, Papadakis M, Labate D. Automated sorting of neuronal trees in fluorescent images of neuronal networks using NeuroTreeTracer. *Sci Rep*. 2018. doi:10.1038/s41598-018-24753-w

102. Feng L, Zhao T, Kim J. neuTube 1.0: A New Design for Efficient Neuron Reconstruction Software Based on the SWC Format. *eNeuro*. 2015;2(1):1-10. doi:10.1523/JNEUROSCI.2055-07.2007

103. Peng H, Ruan Z, Long F, Simpson JH, Myers EW. V3D enables real-time 3D visualization and quantitative analysis of large-scale biological image data sets. *Nat Biotechnol Nat Am Inc*. 2010;28(4):348-353. doi:10.1038/nbt.1612

104. Turrigiano G. Too Many Cooks? Intrinsic and Synaptic Homeostatic Mechanisms in Cortical Circuit Refinement. *Annu Rev Neurosci*. 2011;34(1):89-103. doi:10.1146/annurev-neuro-060909-153238

105. Gipson CD, Olive MF. Structural and functional plasticity of dendritic spines – root or result of behavior? *Genes, Brain Behav*. 2017;16(1):101-117. doi:10.1111/gbb.12324

106. Hersch S, Ciliax B, Gutekunst C, et al. Electron microscopic analysis of D1 and D2 dopamine receptor proteins in the dorsal striatum and their synaptic relationships with motor corticostriatal afferents. *J Neurosci*. 1995;15(7):5222-5237. doi:10.1523/jneurosci.15-07-05222.1995

107. Petreanu L, Mao T, Sternson SM, Svoboda K. The subcellular organization of neocortical excitatory connections. *Nature*. 2009;457(7233):1142-1145. doi:10.1038/nature07709

108. Rane M, Manchanda R. Effects of location and extent of spine clustering on synaptic integration in striatal medium spiny neurons—a computational study. *Med Biol Eng Comput*. 2018;56(7):1173-1187. doi:10.1007/s11517-017-1760-5

109. Ansari AM, Ahmed AK, Matsangos AE, et al. Cellular GFP Toxicity and Immunogenicity: Potential Confounders in in Vivo Cell Tracking Experiments. *Stem Cell Rev Reports*. 2016;12(5):553-559. doi:10.1007/s12015-016-9670-8

110. Detergents: Triton X-100, Tween-20, and More. *Mater Methods*. 2013;3(163).

111. Dresbach T, Hempelmann A, Spilker C, et al. Functional regions of the presynaptic cytomatrix protein Bassoon: Significance for synaptic targeting and cytomatrix anchoring. *Mol Cell Neurosci*. 2003;23(2):279-291. doi:10.1016/S1044-7431(03)00015-0

112. Miklosi AG, Del Favero G, Bulat T, et al. Super-resolution Microscopical Localization of Dopamine Receptors 1 and 2 in Rat Hippocampal Synaptosomes. *Mol Neurobiol*. 2018;55(6):4857-4869. doi:10.1007/s12035-017-0688-y

113. Micheva KD, Busse B, Weiler NC, O'Rourke N, Smith SJ. Single-Synapse Analysis of a Diverse Synapse Population: Proteomic Imaging Methods and Markers. *Neuron*. 2010;68(4):639–653. doi:10.1371/journal.pone.0178059

114. Micheva KD, Smith SJ. Array tomography: A new tool for imaging the molecular architecture and ultrastructure of neural circuits. *Neuron*. 2007;55(1):25-36.

115. Anastasiades PG, Marques-Smith A, Butt SJB. Studies of cortical connectivity using optical circuit mapping methods. *J Physiol*. 2018;596(2):145-162. doi:10.1113/JP273463

116. Petreanu L, Huber D, Sobczyk A, Svoboda K. Channelrhodopsin-2-assisted circuit mapping of long-range callosal projections. *Nat Neurosci*. 2007;10(5):663-668. doi:10.1038/nn1891

Annex I

Mouse strains mentioned in this work:

Common name	Ref	Strain name	Description by Jackson's Laboratory (JAX®) www.jax.org	Alleles of interest for Genotyping
C57BL6/J (WT)	http://jaxmice.jax.org/strain/000664.html	C57BL/6J	C57BL/6J is the most widely used inbred strain and the first to have its genome sequenced. Although this strain is refractory to many tumours, it is a permissive background for maximal expression of most mutations. C57BL/6J mice are resistant to audiogenic seizures, have a relatively low bone density, and develop age related hearing loss. They are also susceptible to diet-induced obesity, type 2 diabetes, and atherosclerosis. Macrophages from this strain are resistant to the effects of anthrax lethal toxin.	$Nnt^{C57BL/6J}$
Tlx3	https://www.mmrrc.org/catalog/sds.php?mmrrc_id=36547	STOCK Tg(Tlx3-cre)PL56Gsat/Mmucd (Hemizygote)	BAC engineering was used to insert an intron containing Cre cassettes, followed by a polyadenylation sequence to terminate transcription of the fusion transcript immediately after the recombinase gene, into the BAC vector at the initiating ATG codon in the first coding exon of the gene.	Cre
OE25	https://www.mmrrc.org/catalog/sds.php?mmrrc_id=36502	STOCK Tg(Chrna2-cre)OE25Gsat/Mmucd (Hemizygote)	BAC engineering was used to insert an intron containing Cre cassettes, followed by a polyadenylation sequence to terminate transcription of the fusion transcript immediately after the recombinase gene, into the BAC vector at the initiating ATG codon in the first coding exon of the gene. The BAC address for this line is RP23-18E12.	Cre
EY217 (D1CRE)	http://www.mmrrc.org/catalog/sds.php?mmrrc_id=30778	STOCK Tg(Drd1a-cre)EY217Gsat/Mmucd (Hemizygote)	These transgenic mice have a modified BAC-Cre injected into pronuclei of FVB/N fertilized oocytes. Hemizygous progeny was mated to non-inbred mice from a mix of B6/129/Swiss/FVB stocks. Mice were sent to NIH/NIMH for testing and NIH/NIMH crossed these with ROSA26-GFP mice to get the desired expression for testing. However, the MMRRC will breed all these strains to C57BL/6J and select for mice with only the Cre expression, eliminating the ROSA26-GFP from each line. Mice distributed from these strains will only have Cre, and not EGFP.	Cre